République algérienne démocratique et populaire
Ministère de l'enseignement supérieur et de la recherche scientifique
Université Saad Dahleb Blida 1

Faculté des sciences
Département de physique

Mémoire de fin d'étude
Pour l'obtention du diplôme de Master en Physique
Option : Micro & Nano Physique

Thème :

# Magnetic and eddy current testing of iron/silicon oxide-based nanocomposites

Présenté par :

**SEBTI Fayza**

Soutenu le 09 /07/ 2023 devant le jury composé de :

| | | |
|---|---|---|
| Dr.AOUDJ SALLAH EDDINE | MCA USDB | Président |
| Dr. OUARAB NOUREDINE | MRA CRTSE | Examinateur |
| Dr. YOUNES ABDERRAHMANE | MRA CRTI | Encadreur |
| Dr. ABDELKADER HASSEIN-BEY | MCB USDB | Co-Encadreur |

Blida 1-2022/2023

## ملخص

تظهر مركبات الحديد - أكسيد السيليكون على نطاق النانو خصائص ممتازة مقارنة بالمواد التقليدية بنفس التركيز بسبب تأثير حجم البلورة. يهدف هذا العمل إلى دراسة التغيرات في السلوك الكهرومغناطيسي والمغناطيسي للمركب النانوي الحديد - السيليكون خلال عملية التحضير. النهج المتبع في هذه الدراسة يتضمن استخدام تقنيات الاختبار غير المدمرة (NDT) بوسائل مغناطيسية لمتابعة تطور الهيكل، والإجهادات المتبقية، والعيوب، والتغيرات المغناطيسية والسلوك الكهرومغناطيسي خلال عملية التحضير. كما يهدف إلى إيجاد علاقة بين التقنيات الهيكلية وتقنيات NDT.

## Résumé

Le nano-composite de fer-oxyde de silicium présente d'excellentes propriétés par rapport aux matériaux conventionnels de même concentration en raison de l'impact de la taille cristalline. Ce travail vise à étudier les changements de comportement électromagnétique et magnétique du nano-composite fer-silicium au cours du processus d'élaboration. L'approche adoptée dans cette étude consiste à utiliser des techniques de contrôle non destructif (CND) par les méthodes magnétiques pour suivre l'évolution de sa structure, des contraintes résiduelles, des défauts, des changements magnétiques et du comportement électromagnétique lors du processus d'élaboration. De plus, il vise à établir une relation entre les techniques structurales et les techniques de CND.

## Abstract

The nano-composite iron–silicon oxide shows excellent properties compared to conventional materials with the same concentration due to the impact of the crystalline size. This work aims to study the changes in the electromagnetic and magnetic behavior of nanocomposite iron–silicon during the elaboration process. The approach adopted in this study implies using non-destructive testing (NDT) techniques by magnetic methods to follow the evolution of its structure, residual stresses, defects, magnetic changes and electromagnetic behavior during the elaboration process. Also, to find a relationship between the structural and the NDT techniques.

# Acknowledgement

*I would like to thank God Almighty for having given me the health, will and patience to start and finish this thesis.*

*Before going any further into the details of this experience, it seems appropriate to begin this with a word of thanks; to those who shared their time and knowledge with me over the years.*

*First of all, this work would not be as rich and would not have been possible without the help and guidance of my supervisors Dr. YOUNES Abderrahmane and Dr. ABDELKADER Hassein-Bey. I appreciate their patience, objectivity and availability during the preparation of this thesis.*

*I would also like to express my sincere thanks to the members of the jury, Dr. AOUDJ Sallah-Eddine and Dr. OUARAB Nouredine, for their kindness in examining and judging this humble work.*

*I would also like to express my gratitude to my teachers in the physics department and the researchers at CRTI Chéraga who contributed to my training.*

*I would also like to thank my family and friends for their support, encouragement and love during all the difficult times, without whom i might not have been able to get here.*

*Finally, I salute all those who have contributed in any way to the realization of this work.*

# Dedication

"*This thesis is lovingly dedicated to the notable individuals who have deeply influenced my journey, enriched my aspirations and motivated me to pursue for excellence.*

*To my dad and mom who gave their lives so i can be the best version of me. To my soulmate fish Lili for being always and forever beside me. To my babies Ahmed, Saif and Biba.*

*To my precious friends Imen, Hanane and all my classmates for sharing joyful moments with me.*

*I extend my heartfelt appreciation to the dearest Boudj and Senpai for being such a valuable support.*

*To all those who have generously contributed, in any capacity, to the realization of this thesis, your encouragement and belief in my abilities have been key in this achievement*."

## List of Figures and Tables:

## Table of Contents:

## General Introduction:

Nanotechnology refers to the manipulation and comprehension of matter on a scale ranging from approximately 1 to 100 nanometers, which leads to distinctive and size-dependent characteristics [1]. This area holds enormous potential for research and development, including modeling, imaging, measurement, and more. Due to its focus on the extremely small, nanotechnology is applicable across multiple research fields and interdisciplinary domains, including but not limited to Engineering, Biology, Electronics, Chemistry, Physics, Medicine, Materials Science, Energy, and Informatics [2].

The development of materials and production equipment by individuals is considered to be the main factor in the observed differences between countries and regions. One method that has received considerable attention for the production of advanced materials is mechanical alloying. This distinctive process allows for the synthesis of new families of advanced materials that are not achievable through alternative methods. With the advantage of operating at room temperature, mechanical alloying facilitates the successful fabrication of a wide range of engineering materials, including nanostructured materials, nanoparticles, nanocomposites, carbon nanotubes, and amorphous and metallic glassy alloys[3].

Fe particles in nanocrystalline form are known for their remarkable magnetic properties, such as high saturation magnetization, permeability, and low coercivity. However, these nanoparticles have a strong affinity for oxygen, which can lead to oxidation. To address this issue, extensive research has been conducted to explore the encapsulation of Fe particles within silica. This approach involves dispersing the Fe nanoparticles in a non-magnetic matrix or coating, effectively protecting them from oxidation while preserving their magnetic characteristics [4, 5]. Iron-silica nanocomposites have garnered significant attention due to their unique properties. These composites exhibit higher resistivity, which when combined with the excellent magnetic properties of metallic Fe, makes them well-suited for dielectric applications. Moreover, Fe-silica nanocomposites hold the potential to serve as a viable alternative to traditional ferrite materials [6].

The main focus of this study is to investigate how the electromagnetic and magnetic properties of the iron-silicon nanocomposite change during its fabrication process. To achieve this, non-destructive testing techniques using magnetic methods are employed. The study aims to give a relation between the structural properties and the non-destructive testing techniques utilized. The obtained powder mixture is subjected to characterization techniques such as SEM, XRD, and finally VSM technique for magnetic determination. By conducting a thorough examination of the alloy's properties, this study aims to contribute to the understanding of nanocomposite materials and provide valuable insights for potential applications in various fields.

The thesis is divided into three chapters:

- ✓ Chapter 1: Provides an overview of nanomaterials and nanocomposites, with a particular emphasis on mechanosynthesis and its parameters. It also presents various relevant research studies conducted on the alloy.
- ✓ Chapter 2: Explains the methodology and characterization techniques employed to analyze the powder mixture.
- ✓ Chapter 3: Describes the findings of the study and provides an interpretation of the results obtained.

Finally, a conclusion that provided valuable insights into the fabrication and characterization of the iron-silicon nanocomposite. As well as the obtained results that highlights the advancements achieved in understanding the electromagnetic and magnetic behavior of such nanocomposites and what it can contribute to the field of nanotechnology.

# CHAPTER 1

## A comprehensive overview of nanocomposite materials

# 1. Nanotechnology and Nanomaterials :

## 1.1. Introduction :

The remarkable advancements in technology owe much to the emergence of nanomaterials, which offer tunable physical, chemical, and biological properties with enhanced functionality. These materials are typically classified based on factors such as their size, composition, shape, and source, and the ability to predict their distinct properties has become a valuable asset in any classification scheme [7].

It is presently an era of research that is often referred to as the age of nanoscience and nanotechnology. The notion of nanomaterials has garnered significant attention from scholars, researchers, and scientists due to their distinct properties that set them apart from their bulk material counterparts, making them increasingly popular in the research community [8].

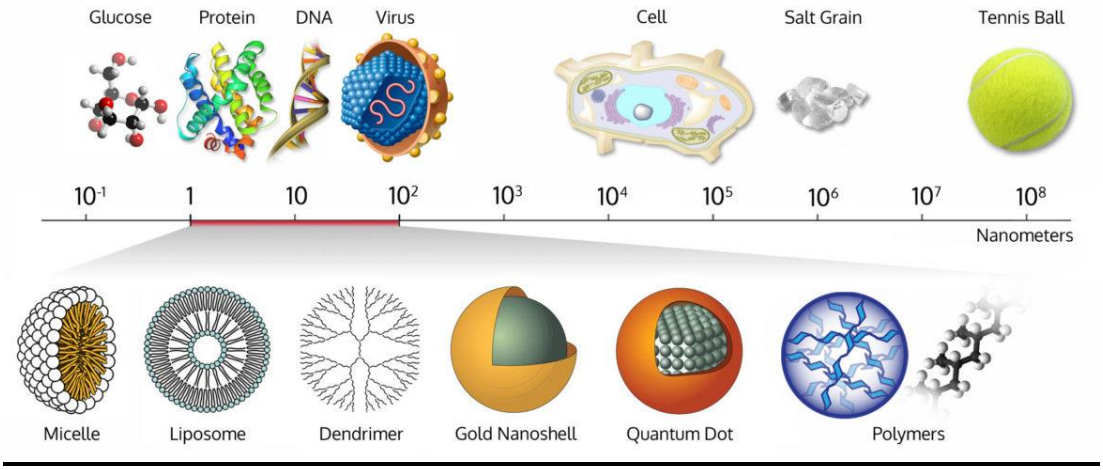


Figure 1.1: nanotechnology chart ruler [9].

## 1.2. History of nanotechnology and material science :

The term nanometer was initially introduced in 1914 by Richard Adolf Zsigmondy, while the concept of nanotechnology was formally introduced by American physicist and Nobel laureate Richard Feynman during his address at the American Physical Society's annual meeting in 1959. In his speech, Feynman envisioned the development of machines at the molecular level, stating, ‘‘*why can’t we write the entire 24 volumes of the*

*Encyclopedia Britannica on the head of a pin*?'' Consequently, he is widely recognized as the father of modern nanotechnology. However, it is believed that Norio Taniguchi was the first to use the term "nanotechnology" in 1974, describing it as '' *nano-technology mainly consists of the processing of, separation, consolidation, and deformation of materials by one atom or one molecule*'' . Interestingly, the use of nanomaterials dates back to ancient times, with humans utilizing asbestos nanofibers to reinforce ceramic composites over 4,500 years ago. The ancient Egyptians also employed PbS nanoparticles over 4,000 years ago in their hair dye recipes. Another fascinating example from the past is the Lycurgus Cup, a dichroic cup created by the Romans in the 4th century that appears jade-like in direct light and translucent ruby in transmitted light. The cup's color variations are due to the presence of Ag and Au nanoparticles [10].

The first transistor was created in 1947 by Bardeen, Brattain, and Shockley, and they were awarded the Nobel Prize in 1956 for their pioneering work. The development of silicon-based transistors followed in 1951, and by 1958, the integrated circuit had been invented. In 1965, Gordon E. Moore was a founding member of Intel and proposed what is now known as Moore's Law. In 1965, a chip contained 30 transistors, which had increased to 2,000 by 1971 and now exceeds 40,000 transistors. According to the National Nanotechnology Initiative (NNI), scaling down the transistor size to 9 nm or smaller will result in the production of chips with billions of transistors [8].

## 1.3. Nanocomposites :

Due to their improved quality compared to simple metal nanoparticles, scientists have recently been interested in nanocomposite materials. To create new types of materials, several materials, some of which can range in size from 1 to 100 nm [11], are combined to form nanocomposites. As a result, nanocomposite materials can have mechanical, electrochemical, electrical, catalytic, thermal and optical properties that are markedly different from the component materials [12-15].

Nanocomposites exhibit various phases, including non-dimensional (core-shell), one-dimensional (nanowires and nanotubes), two-dimensional (lamellar), and three-dimensional (metal matrix composites). These phases are based on the structural characteristics of the nanocomposites, such as nanolayer composites, nanofiber composites, and nanoparticle composites [16].

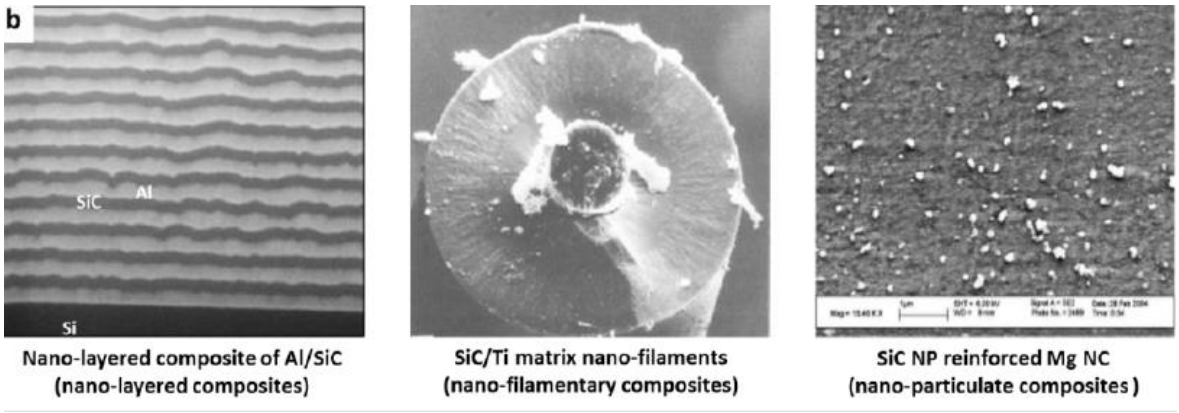


Figure 1.2: The three identifications of Nanocomposites [17].

Nanocomposites have attracted the attention of scientists, researchers and engineers, leading to an increase in research publications on these materials. These materials have emerged as the materials of the 21st century, leading to a series of technological and commercial breakthroughs in various industries and fields [17].

## 1.4. Nanocomposites classification :

Similar to microcomposites, nanocomposite materials can be categorized into three distinct groups based on their matrix materials [18]:

### 1.4.1 Ceramic matrix nanocomposites (CMNCs) :

Ceramic matrix nanocomposites (CMNCs) are advanced materials that combine one or more separate ceramic phases to improve wear resistance, thermal stability, and chemical stability. They typically consist of a matrix in which energy-dissipating components such as fibers, platelets or particles are embedded to reduce brittleness and increase breaking strength [19].

There are various methods being developed for synthesizing CMNCs, with the latest techniques focusing on single-source precursor methods based on melt-spinning composite precursors followed by fiber treatment and pyrolysis [20]. However, older methods also exist [21], such as: conventional powder method; polymer precursor route; spray-pyrolysis; vapor techniques (CVD and PVD). Chemical methods include: sol-gel process; colloidal and precipitation technique; the template synthesis.

Tableau 1.1: Processing methods for CMNC [22].

| Method | System |
|---|---|
| **Powder process** | $Al_2O_3$/SiC |
| **Polymer precursor process** | $Al_2O_3$/SiC, SiN/SiC |
| **Sol-gel process** | $SiO_2$/Ni, ZnO/Co, $TiO_2/Fe_2O_3$, $La_2O_3/TiO_2$, $Al_2O_3/SiO_2$, $NdAlO_3/Al_2O_3$ |

### 1.4.2 Metal matrix nanocomposites (MMNCs) :

Metal matrix nanocomposites (MMNCs) are advanced materials consisting of a metal matrix or a ductile alloy reinforced with nanoscale materials. MMNCs are known for their outstanding properties including high ductility, strength, toughness and modulus making them ideal for various applications such as the aerospace and automotive industries [18].

The preparation of MMNCs involves several techniques, with the most commonly used ones being: spray pyrolysis , liquid metal infiltration , rapid solidification , vapor techniques (PVD, CVD), electrodeposition and chemical methods, which include colloidal and sol-gel processes [23-27].

Tableau 1.2: Processing methods for MMNC [22].

| Method | System |
|---|---|
| **Spray pyrolysis** | W/Cu, Fe/MgO |
| **Liquid Infiltration** | Pb/Cu, W/Cu/ Nb/Cu, Pb/Fe Nb/Fe, Al- C60 |
| **Sol-gel** | Fe/SiO2,Ag/Au, Au/Fe/Au |
| **Rapid solidification process** | Al/X/Zr (X = Si, Cu, Ni), Al/Pb, Fe alloy |
| **RSP with ultrasonics** | Al/SiC |

### 1.4.3 Polymer matrix nanocomposites (PMNCs) :

In polymer matrix nanocomposites (PMNCs), the nanofillers, also called nanocomponents, are typically fillers that can be categorized into three types based on their morphology: 1D-linear (such as carbon nanotubes), 2D-layered (such as montmorillonite), and 3D-powder (such as silver nanoparticles) [28]. The production of PMNCs can be

achieved through methods similar to those used for typical composites, such as in-situ, solvent methods, or mixing a molten polymer matrix. PMNCs exhibit several desirable characteristics, including high thermal stability, improved mechanical properties (such as high abrasion resistance), and lower air permeability (which results in a higher barrier capacity) [29]. Numerous methods have been employed for the preparation of polymer nanocomposites, with the most widely used methods being [30] :

– Intercalation of the polymer or pre-polymer from solution ;
– In-situ intercalative polymerization ;
– Melt intercalation ;
– Template synthesis (Sol-gel technology).

## 1.5. Applications of Nanocomposites :

Nanocomposites have been demonstrated to provide numerous benefits such as enhanced properties, decreased solid waste (through lower film thickness and reinforcement usage), and improved manufacturability, particularly in the field of packaging applications. Additionally, the potential applications of nanocomposite systems are vast, including the creation of new materials and the enhancement of the performance of established devices such as fuel cells, sensors, and coatings. While the industrial utilization of nanocomposites is presently limited, their transition from research to industry has already begun and is projected to be substantial in the near future [22].

The use and demand for nanocomposites has increased rapidly, leading to a significant boost in their applications. Global production of nanocomposites is projected to exceed 600,000 tonnes over the next decade, with significant growth expected in the following regions [31]:

- Superior strength fibers and films
- UV protection gels
- Drug delivery systems
- New fire retardant materials
- Anti-corrosion barrier coatings
- Lubricant and stretch paints

Nanocomposites have received considerable interest in the automotive and industrial sectors due to their ability to improve mechanical properties. They are now used in a wide variety of vehicles including engine covers, door covers and timing belt covers. In addition, they are also used in the manufacture of vacuum cleaner blades, mower hoods, cell phone cases, and more [31].

## 1.6. Nanocomposites properties :

The properties of nanocomposites depend on a variety of factors, including the type, size, shape, and concentration of the nanoparticles, as well as the properties of the matrix material. nanocomposites offer a wide range of properties that can be tailored to meet the specific needs of different applications. Some general properties of nanocomposites are [32]:

- **Electrical property :**

Polymer nanocomposites are being developed as lightweight materials with potential applications in electrostatic discharge, electrical interconnects, conductive coatings, and electromagnetic shielding with conductivities tailored between $10^{-6}$ to 100 S cm−1. Nanotubes and metallic nanorods are typically dispersed in polymer matrices for the development of conductive nanocomposites. The critical issues include the development of percolative structures, the formation of hierarchical structures, the orientation state of nanoparticles, and the junction resistance between matrix and nanoparticle and between nanoparticles. Metallic nanorods can demonstrate a dielectric strength in excess of $10^5$ at concentrations (and orientations) that are close to the percolation, which could result in their use in ultrahigh capacitors. Pristine layered silicates with charge-balancing cations have been suggested as possible motifs for single ion conductors for potential Li-ion battery applications [33,34].

- **Mechanical property :**

Fillers added to the matrix can change the mechanical properties of the matrix material. For conventional composite materials, theories of micromechanics suggest that the overall mechanical properties of the composite are functions of the properties of the components, of the volume fraction of the components, of the shape and orientation of the inclusions and of the dispersion state. It does not consider interactions between charges and matrices at their interface. For nanocomposites, the improvement of mechanical properties

depends not only on the above factors, but also on the interaction between the filler and the matrix [15].

- **Magnetic properties :**

There are two types of NC compounds exhibiting magnetic properties, one containing metallic NPs and the other containing ferrite NPs. Essentially, the lack of hysteresis indicates increased superparamagnetic activity in the ferrite NPs. The nanocomposite containing a concentration of 2.8% ferrite was found to have no hysteresis at room temperature and was clearly visible. They also found that the nanocomposite containing $\gamma$-$Fe_2O_3$in the electromagnetic polymer matrix did not exhibit hysteresis. Nanoparticles from the synthesis of nickel oxide in polyvinyl cinnamate also exhibit magnetic properties. They found a ferromagnetic state in nickel nanomaterials. In addition, the values of weight gain, magnetic reactivity and hysteresis were obtained when incorporating nickel oxide NPs on nanocomposite materials [35].

The importance of magnetic properties extends to different technologies and can be used in various fields. These properties come from quantum effects related to spin interactions. However, most materials have zero net magnetization due to the presence of regions of magnetization known as domains. The distribution of magnetization direction in these domains is random, resulting in negligible net magnetization [36].

## 1.7. Magnetic Nanocomposites :

Magnetic nanocomposites are composites consisting of nano-sized magnetic materials that can be activated by an external stimulus, such as a static magnetic field or an alternating magnetic field. The researchers combined various materials, such as gels, liquid crystals, renewable polymers, silica, carbon or metal-organic structures, with different types of magnetic particles to search for new nano synthesis. These combinations offer a wide range of possibilities for both basic research and practical applications, including medical therapy and diagnostics, separation, actuation and catalysis [37].

### 1.7.1 Magnetism and hysteresis :

The emergence of magnetism traced back to the earliest days of scientific research, making the history of magnetism inseparable from the history of science. We show some magnetism ages in the following table [38]:

Tableau 1.3: The seven ages of magnetism.

| Period | Dates | Icon | Drivers | Materials |
|---|---|---|---|---|
| **Ancient period** | -2000-1500 | Compass | State, geomancers | Iron, Iodestone |
| **Early modern age** | 1500-1820 | Horsehoe magnet | Navy | Iron, Iodestone |
| **Electromagnetic age** | 1820-1900 | Electromagnet | Industy/ infrastructure | Electrical steel |
| **Age of understanding** | 1900-1935 | Pauli matrices | Academic | (Alnico) |
| **High-frequency age** | 1935-1960 | Magnetic resonance | Military | Ferrites |
| **Age of appmications** | 1960-1995 | Electric screwdriver | Consumer market | Sm-Co, Nd-Fe-B |
| **Age of spin electronics** | 1995- | Read head | Consumer market | Multilayers |

The most prominent manifestation of magnetism in solids is the spontaneous magnetization of ferromagnetic materials such as iron or magnetite. Spontaneous magnetism is often associated with hysteresis, a phenomenon studied by James Ewing and named by him in 1881 [38].

The hysteresis loop characterizes the behavior of a ferromagnet subjected to an external magnetic field. Initially.

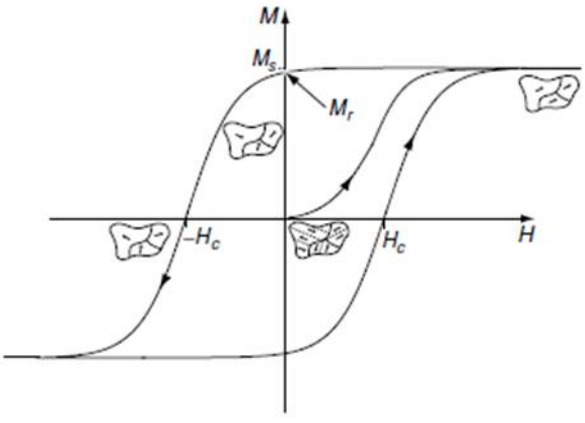


Figure 1.3: The ferromagnetic hysteresis loop [38].

the ferromagnet is in an unmagnetized, virgin state, with no net magnetic moment. As the magnetic field H is applied, it modifies and eventually eliminates the microstructure of ferromagnetic domains magnetized in different directions, until the spontaneous

magnetization $M_s$ is revealed. The loop shows the evolution of the magnetization as H is increased and then decreased back to zero [38]

Two important parameters of the loop are the remanence $M_r$, which is the residualmagnetization after the external field is removed, and the coercivity $H_c$, which is the minimum reverse field required to reduce the magnetization to zero [38].

- ✓ Hard magnetic materials have broad, square M(H) loops and are ideal for permanent magnets as they stay magnetized even when the field is removed.
- ✓ Soft magnetic materials have narrow loops and are temporary magnets that lose their magnetization as soon as the field is removed.

### 1.7.2 Domains of magnetism :

- **Diamagnetic Material :** Diamagnetic materials exhibit negative magnetism, repelling external magnetic fields by producing an internal field in opposite polarity. The material conducts the external field around it, rather than through it, with a permeability less than one and negative [36].

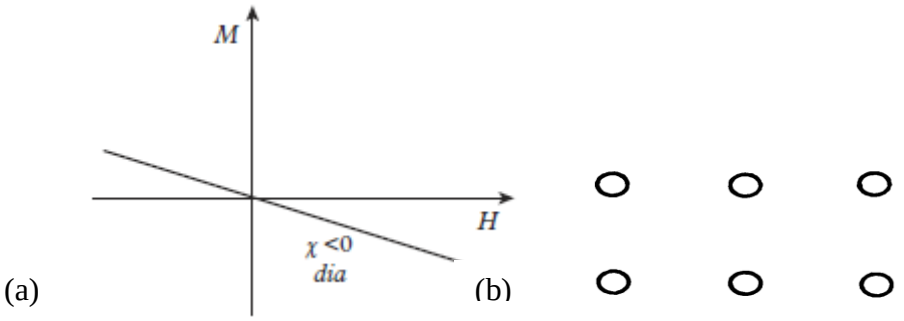


Figure 1.4: (a) Magnetization, M, as a function of the applied field, H. (b) the magnetic structure of diamagnetism (no inherent magnetic moments.) [39, 40].

- **Paramagnetic Material :** Paramagnetic materials have a permeability less than 1, allowing magnetic fields to pass through them with less resistance. They can undergo partial magnetization when they are subjected to an external magnetic field, due to the polarization of random moments cause of thermal agitation [36].

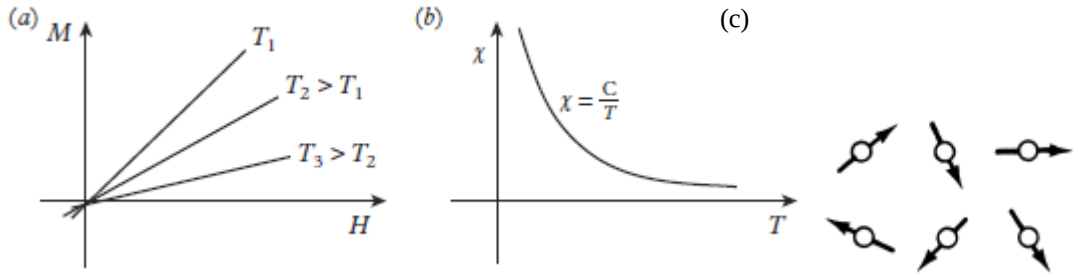


Figure 1.5: (a) Magnetization, M, as a function of the applied field, H. (b) χ versus T, the Curie law of paramagnetism.(c) the magnetic stucture of paramagnetism [39,40].

- **Ferromagnetic Material :** Ferromagnetic materials are distinguished from other materials by their ability to conduct flux higher than free space because their permeability is greater than one. This property makes them attract magnetic flux relative to free space. The three elements that exhibit ferromagnetism are iron, cobalt, and nickel [36].

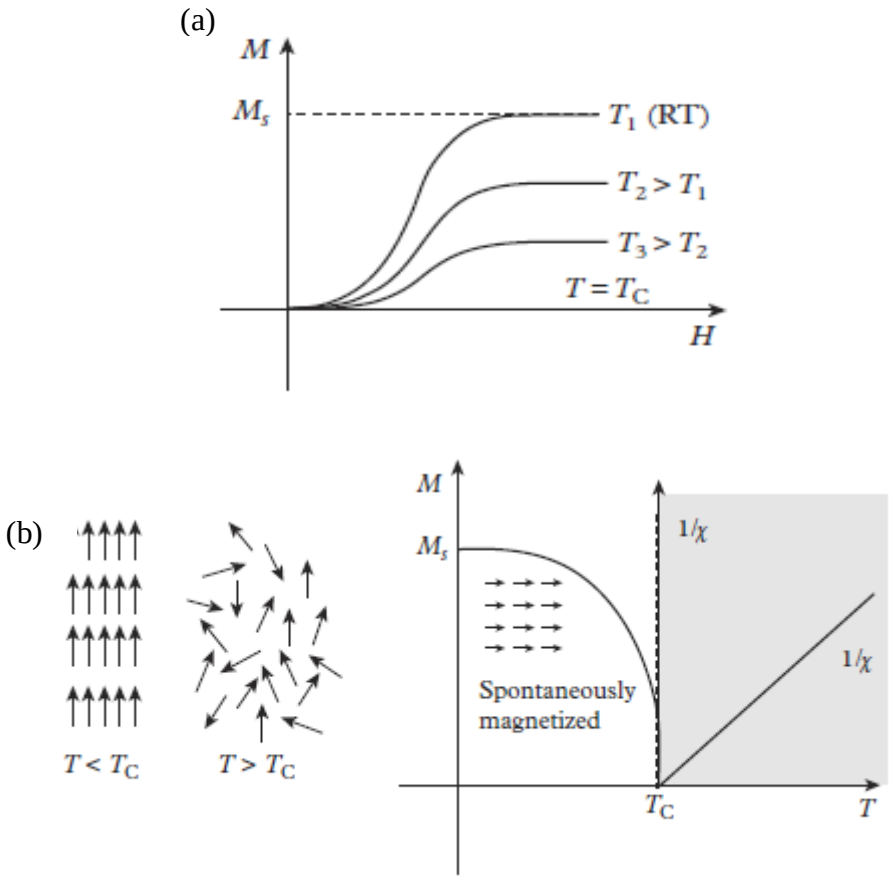


Figure 1.6: (a) Initial magnetization of a ferromagnet as a function of applied field and temperature. (b) Magnetization of a ferromagnet as a function of temperature [39].

- **Antiferromagnetic Material and Ferrimagnetic Material :** Antiferromagnetic materials require a specific temperature, known as the Neel temperature, to become permeable. The permeability of these materials is generally less than 1. Ferrimagnetic materials are naturally occurring materials such as iron ore and nickel ore that possess an overall magnetic flux [36].

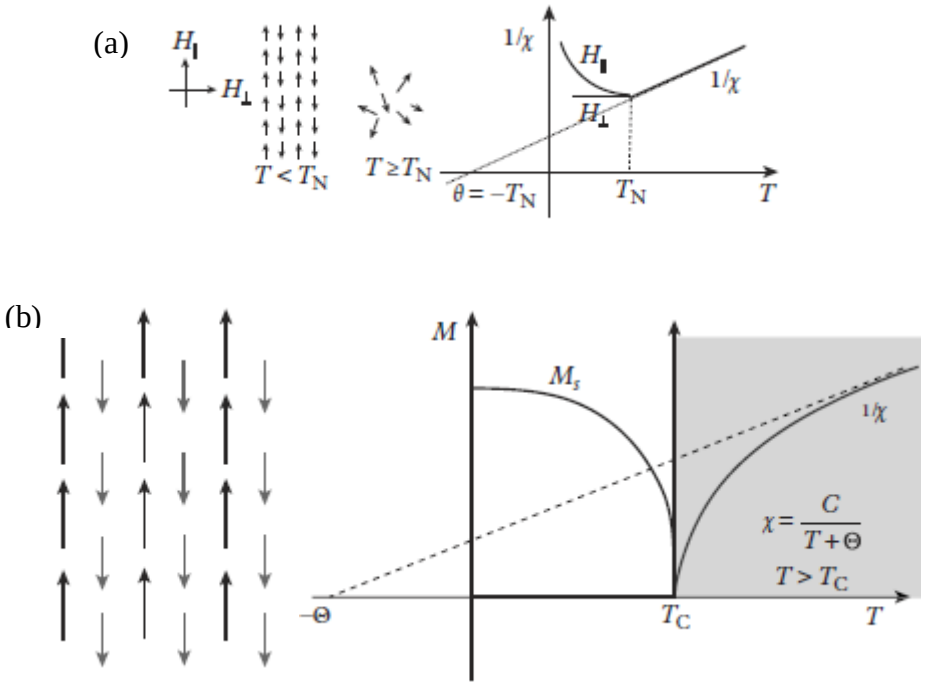


Figure 1.7: (a) Magnetization behavior of an antiferromagnetic material as a function of temperature. (b) Magnetization of a ferrimagnet as a function of temperature [39].

## 1.8. Nanocomposites Synthesis :

To obtain materials with specific structural, mechanical, optical, magnetic or electronic properties, it is necessary to promote engineering nanofabrication methods that allow precise control at the atomic scale in material development and processing. It is devided into two major categories [41] :

- **Top-down approach** : The process entails utilizing external experimental parameters to control nanofabrication tools and create nano-sized structures and functional devices with targeted shapes and properties. This is accomplished by beginning with larger dimensions and scaling them down to achieve the desired size.

- **Bottom-up approach** : The objective is to construct complex nanoscale assemblies, or directed self-assemblies, by arranging molecular or atomic components through the use of advanced mechanisms and technologies.

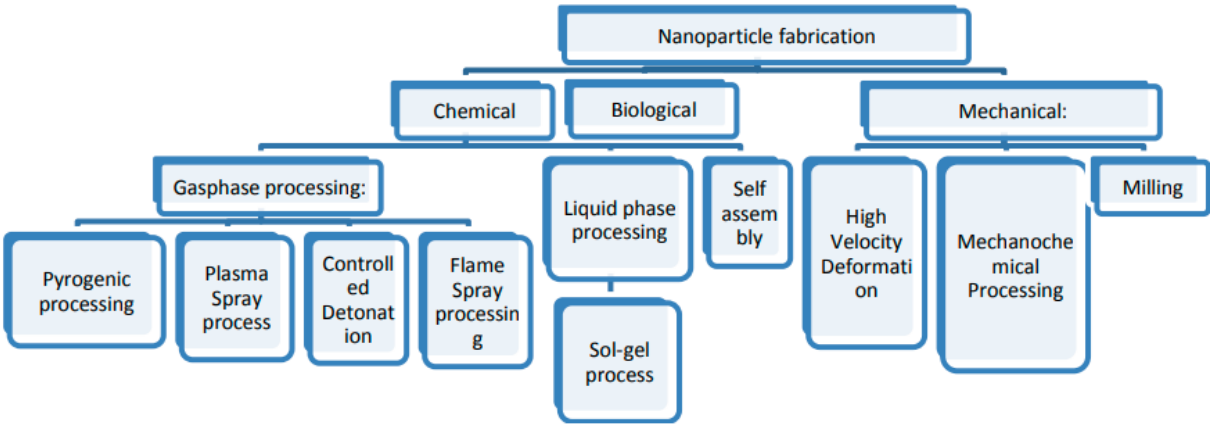


Figure 1.8: Methods of fabrication for nanomatrials [42].

As previously mentioned, each group of nanocomposites requires a specific fabrication technique. This information is summarized in the figure provided below.

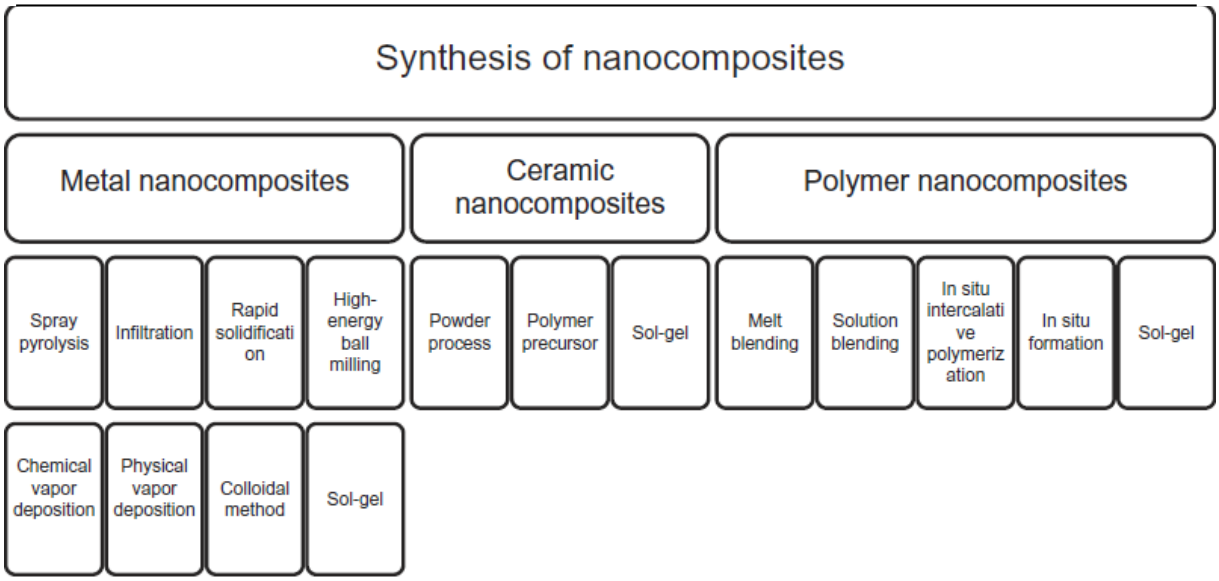


Figure 1.9: Nanocomposite fabrication techniques [43].

## 1.9 Mechanosynthesis :

Mechanosynthesis is an efficient approach to fabricate nanoscale materials by facilitating various solid-state reactions. It allows direct synthesis of intermetallic compounds, carbides, arsenides, silicides from powders of elements or compounds and elements. The process also enables the reduction of oxides and sulfides, mixing and exchange reactions leading to the formation of various nanocomposites [44]. Advances in scientific materials research have led to the development of a wide variety of complex materials through new preparation methods over the past few decades [45].

In this study, the intrest is on the Top-down approaches specifically the mechanical milling.

### 1.9.1 Mechanical Alloying :

Mechanical alloying (MA) is a solid-state powder processing technique that was first developed more than 50 years ago by John Benjamin of INCO. Its original purpose was to produce a material with sufficient strength at both intermediate and elevated temperatures. In recent years, MA has become recognized as a crucial method for synthesizing various metastable materials, including supersaturated solid solutions, intermetallics, quasicrystalline phases, nanocrystalline materials and nanocomposites, amorphous alloys, and high-entropy alloys. It is generally accepted that the formation of alloy phases during MA from blended elemental powders is due to the creation of a very fine and intimate mixture of the components after milling, if not the final product [46].

### 1.9.2 Alloying Process :

In mechanical milling, ball-powder-ball collision is the main event. When the balls collide, the powder particles are trapped between them and undergo deformation and/or fracture processes to determine the final powder structure. The powder components can be classified into different categories for convenience [47] :

**a. Ductile - Ductile Components :**

Benjamin and Volin (1974) were the first to provide a phenomenological description of mechanical milling of ductile and ductile-brittle components. They described the process as a competition between cold-welding and fracture. The mechanical alloying process was divided into five sequences based on observations of the powders at various

stages of milling using optical microscopy. During the initial stage, micro-forging flattens ductile powders into plates and fragments brittle components into finer particles. Extensive cold-welding follows, resulting in a composite lamellar structure of the ductile components. At longer milling times, the composite powder particles are further refined, and alloying begins. With continued milling, components that exhibit complete solid solubility mix to the atomic level. The enhanced diffusion paths of the lattice defects created by deformation, any heating introduced during milling, and the shortened diffusion paths as the lamellae become finer and more convoluted contribute to the alloying process[48].

**b. Ductile- Brittle Components :**

In a mechanical milling system, the ductile metallic particles such as Ni or Al are flattened and welded together, while the brittle phase such as oxide particles is fragmented and embedded within the layers of the ductile phase. As milling continues, the layers of the ductile phase come closer and eventually merge, while the brittle phase is uniformly distributed as fine particles within the ductile phase matrix. For instance, ball milling of brittle amorphous B with Fe did not lead to alloying, and the B particles remained dispersed in the ductile Fe matrix. In contrast, alloying was observed in the Fe-Si system. To achieve alloying during milling of ductile/brittle components, the brittle component must be fragmented to a small size to shorten diffusion distances and also possess some equilibrium solubility in the ductile phase [49].

**c. Brittle - Brittle Components :**

One might assume that mechanical alloying of brittle/brittle systems would not occur and that the milling process would only reduce the size of the brittle powder components until they reach the limit of comminution. However, mechanical alloying has been achevée at sub-ambient temperatures in ductile/ductile systems (such as NiTi at -40°C). This could be due to the longer diffusion distances required in brittle/brittle systems because of their geometrical differences, and/or the enhanced diffusion paths provided by severe plastic deformation in ductile/ductile systems. Although the mechanism for mechanical alloying in brittle/brittle systems is not well understood, it is evident that material transfer can occur between the brittle components [50].

### 1.9.3 Types of Ball Mill :

There are different types of ball mills, such as drum ball mill, jet ball mill, bead mill, horizontal rotary ball mill, vibrating ball mill and planetary ball mill. These mills can be classified into two types according to their rotational speed: high energy ball mills and low energy ball mills. The choice of ball mill type depends on the specific grinding purpose[45].

As the intrest is on the high energy ball mills lets go through the diffrent equipment types of this technique.

- **planetary ball mill :**

The milling process involves two vials rotating independently around their own axis as well as the line of symmetry of the plate. The movement of the balls inside the vial is driven by the combined effects of Coriolis and centrifugal forces, leading to impacts that impart shear and compressive forces onto the powder particles. These forces induce changes in structure, microstructure, and mechanochemical transformations [51,52].

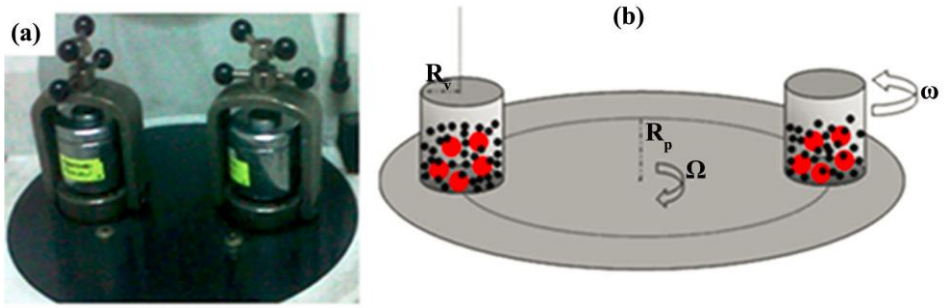


Figure 1.10: (a) Photograph of the two vials on the supporting disc and (b) schematic representation of the experimental planetary ball mill [53].

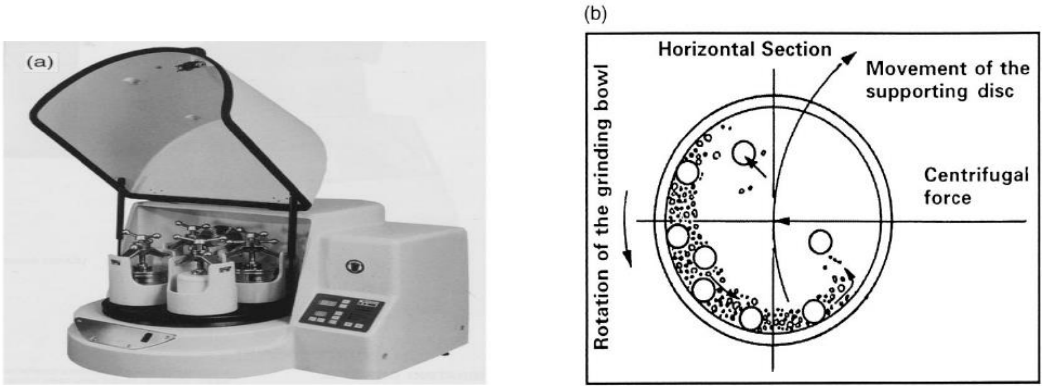


Figure 1.11: (a) Fritsch Pulverisette P-5 four station ball mill. (b) Schematic depicting the ball motion inside the ball mill. Courtesy of Gilson Company, Inc., Worthington, OH[54].

- **Attritor ball mill :**

the Attrition process utilizes free-moving beads to comminute starting materials, while Milling involves an agitator with horizontal arms attached to a vertical rotating central shaft at a speed of 75 to 500 revolutions per minute. Certain high-speed attrition mills can operate at rates between 400 to 2000 revolutions per minute, and during milling, the powders are subjected to pressure from the milling media through impact and shearing[45].

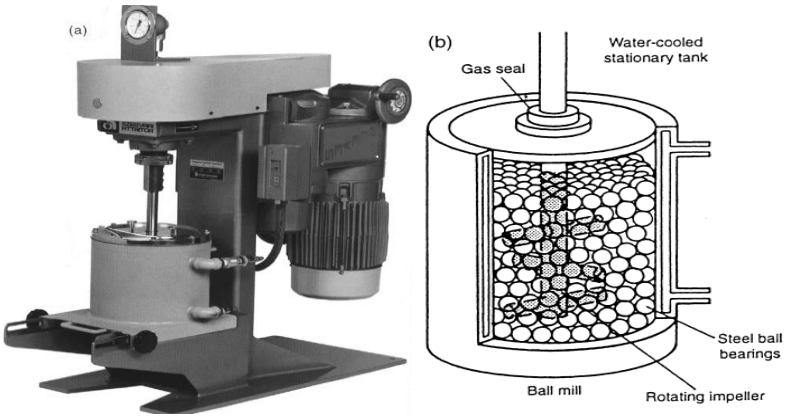


Figure 1.12: (a) Model 1-S attritor. (b) Arrangement of rotating arms on a shaft in the attrition ball mill. Courtesy of Union Process, Akron, OH[54].

- **Shaker ball mill :**

SPEX CertPrep, Inc. in Metuchen, NJ, USA, produces the SPEX shaker mill, which has two models: the Spex 8000M and the Spex 8000D. The first model has a single vial suspended in an arm that oscillates rapidly along multiple axes, while the second model has two vials suspended in two arms. At approximately 1200 rpm, the mill agitates the powder by means of the balls' movements in three perpendicular directions [45].

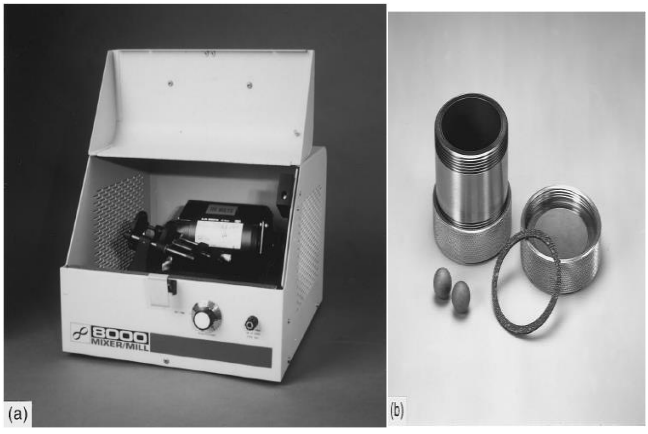


Figure 1.13: (a) SPEX 8000 mixer/mill (b) Tungsten carbide vial set consisting of the vial, lid, gasket, and balls. Courtesy of SPEX CertiPrep, Metuchen, NJ [54].

### 1.9.4 Milling Variables :

The process of Mechanical Alloying requires the optimization of various variables to attain the desired product phase and/or microstructure. Several crucial parameters, such as those listed below, impact the final constitution of the powder [54].

**Type of mill:** There are various types of milling equipment that are available, each with their unique capacity, efficiency, and arrangements for heat transfer and particle removal [55].

**Milling container:** The choice of container material is very important because the impact of the grinding medium on its inner wall may result in some of its material being mixed into the powder. This can lead to contamination or change the chemical composition of the powder [55].

**Milling speed:** The optimal speed should be sufficient only for the balls to descend from their peak height, resulting in the highest possible collision energy [55].

**Milling time:** The crucial factor in the HEBM process is the milling time, which must reach a steady state of fracturing and/or cold welding of powder particles. The required milling time is influenced by the mill type, milling intensity, ball-to-powder ratio, and milling temperature. However, it's crucial to avoid excessively long milling times, as contamination levels increase and undesired phases may form [56].

**Grinding medium:** The characteristics of the grinding medium are essential for efficient milling. The medium's type, size, and distribution all have an impact. High density is necessary to create enough impact force on the material. Large-sized medium is beneficial due to its weight and increased energy transfer. However, using balls with different diameters can result in the highest collision energy [55].

**Milling atmosphere:** Controlling the atmosphere of the grinding vial is an effective means of preventing contamination, particularly for metals susceptible to oxidation. In addition, utilizing different gases in the vial atmosphere can enable the production of compounds like nitrides (using a nitrogen atmosphere) or hydrides (using a hydrogen atmosphere) [57,58].

**Process control agent:** PCAs are commonly used during milling to reduce the effect of cold welding and inhibit agglomeration by adsorbing on the surface of powder

particles. Popular PCAs include stearic acid, hexane, methanol, and ethanol, with a recommended level of 1-5 wt% of the total powder charge [55].

**Temperature of milling:** The temperature of milling significantly affects the formation of various phases and structures, particularly those involving diffusion processes. Temperature can increase during milling due to kinetic energy and exothermic reactions. Cryomilling, or milling at low temperatures, is often used to minimize welding because of the increased brittleness of powder particles [59,60].

**Ball-to-powder weight ratio :** The ratio of ball weight to powder weight (BPR or CR) is an important parameter in milling. Researchers have used a range of BPRs from 1:1 to 220:1. Typically, a BPR of 10:1 is common in small capacity mills like SPEX. However, for large capacity mills like attritors, a higher BPR of up to 50:1 or 100:1 is used[54].

**Extent of filling the vial :** To facilitate alloying of powder particles through impact forces, the milling container must provide sufficient space for both the balls and powder to move around freely. The filling level of the vial with the balls and powder is crucial, as too little material reduces the production rate, while too much reduces the energy of impact. It is recommended to leave around 50% of the vial space empty to avoid overfilling [61,62].

## 1.10 Several studies and researches on $Fe/SiO_2$ alloys :

In 1999, C. de Julián et al aimed to investigate the phase distribution in samples containing Fe nanoparticles dispersed in silica. The researchers prepared $Fe_x/ (SiO_2)_{1-x}$ samples (where x represents the volume percentage, x=0.3 and 0.4) by using high-energy mechanical grinding of Fe particles (average diameter of 60 lm, 99.99% purity) and highly porous amorphous $SiO_2$ gel. Mixtures of these precursor materials were milled under Ar atmosphere, using hardened stainless-steel jars and balls for milling times ranging from 5 to 70 h. The magnetic properties of the samples were studied using SQUID and VSM magnetometers. The coercive force associated with the samples increased with milling time and reached saturation values at around 30 h (550 Oe for the x=0.3 sample and 400 Oe for the x=0.4 sample). The coercivities obtained were higher than the Fe anisotropy field, indicating that the magnetization reversal was governed by an anisotropy different from the bulk Fe magnetocrystalline anisotropy [63].

High energy ball milling was used to prepare Nanocomposite $Fe_{x/}(SiO_2)_{1-x}$ samples by CaoShui Xiong et al in 1999, which were then studied for their microstructure and magnetic properties. X-ray diffraction (XRD), transmission electron microscopy (TEM), Mössbauer spectroscopy, and magnetic balance were used to analyze the samples over a wide temperature range. The results showed a close relationship between the microstructure and magnetic properties of the samples with different Fe contents and ball milling time. Samples with Fe content below 20 wt% and ball milling time of 80 hours exhibited a complex microstructure consisting of small a-Fe grains, Fe clusters implanted in the $SiO_2$ matrix, and nanometer-scale sandwich network-like structures. The nanocomposite $Fe_{x/}(SiO_2)_{1-x}$ samples also showed changes in magnetic properties, which were attributed to their unique nanostructure, grain size effect, strong interface interaction, and interface-osmosis effect at the Fe-$SiO_2$ boundaries [64].

By the year 2000 M. Alonso-Sañudo et al ,conducted a study on the reversal mechanisms of Fe nanoparticles embedded in silica with varying Fe concentrations (x=0.2 to 0.6) below and above the percolation threshold. They used magnetic viscosity and irreversible susceptibility measurements to compare magnetization and demagnetization processes of the samples, which were milled for 24, 48 and 60 hours. The resulting Fe/SiO2 nanoparticulated granular solids exhibited large coercivities and mean switching fields between 600 and 1200 Oe. The study revealed that the high switching fields cannot be explained by a simple coherent reversal model or simple blocking processes of superparamagnetic particles. Instead, full particles were involved in the reversal mechanism aided by dipolar fields of a few hundred Oersted [65].

In 2002 a series of $Fe_x/(SiO_2)_{1-x}$ nanocomposites with x values ranging from 0.2 to 0.6 were prepared by J.J. Blackwell et al using a high-energy milling process for 24, 40, and 60 hours. The resulting Fe/SiO2 nanocomposites exhibited coercivities in the hundreds of Oe. Analysis of their size frequency distributions (SFDs) and magnetic interactions revealed that the switching mechanisms were independent of the Fe concentration. Based on these findings, we proposed a switching mechanism involving avalanches triggered by the reversal of individual particles [66].

G. Pozo López et al by the year 2004 presented initial findings on the structure and magnetic properties of nanocrystalline alloys produced through mechanical alloying using high-energy ball milling to synthesize Fe-dispersed nanocomposites in a silica matrix. A

50 wt% Fe and 50 wt% $SiO_2$ powder mixture was subjected to mechanical alloying for 80 hours at a ball-to-powder weight ratio of 10:1 and a rotation speed of 200 rpm in normal atmosphere. Annealing at 900-1000°C consistently produced the highest coercivity for $SiO_2$/Fe powders. X-ray analysis was performed using a Philips PW 3830 diffractometer with Cu Kα radiation (λ=1.5418 Å), and magnetic properties were evaluated at room temperature using a vibrating sample magnetometer (VSM) LakeShore 7300 with a maximum applied field of 1.5 kOe. Sample S40, which was milled for 40 hours, was studied at 1000°C in air (sample S40air), and thermal analysis was conducted on S40 in argon atmosphere (sample S40ar). X-ray analysis revealed the presence of $SiO_2$ (25.9 wt%), Fe (56.7 wt%), $Fe_2SiO_4$ (fayalite) (13.7 wt%), $Fe_3O_4$ (3.7 wt%), and an unidentified phase. Hysteresis loops for samples S40, S40air, and S40ar are presented in the figure below [67].

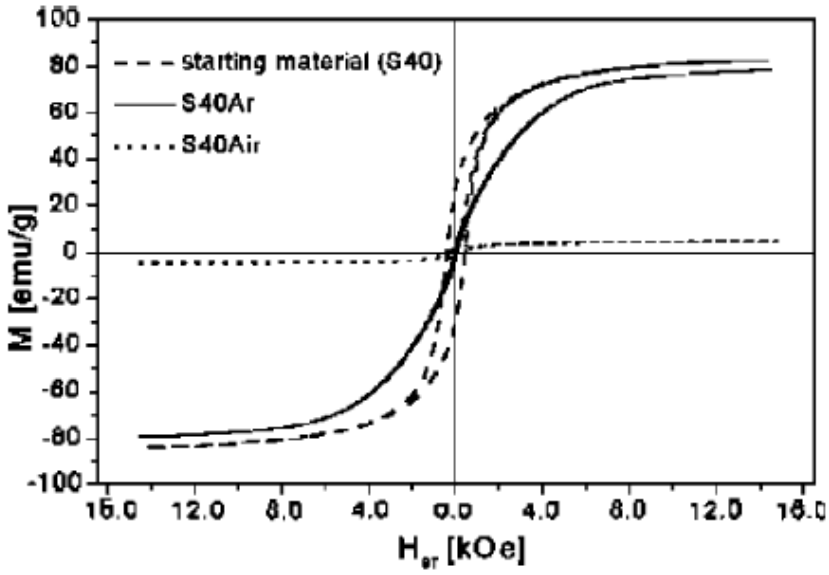


Figure 1.14: Hysteresis loops of sample milled 40 h (S40) and its heat treatments at 1000 1C, in air and argon atmosphere for 1 h [67].

Fe nanoflakes and Fe/$SiO_2$ core-shell nanoflakes were prepared by Longgang Yan et al the year 2010 using a Stober process. Fe nanoflakes were added to a mixture solution of anhydrous ethanol and water, followed by the addition of ammonia solution and tetraethyl orthosilicate. The resulting product was washed with anhydrous ethanol and dried. Sample A and Sample B refer to Fe nanoflakes and Fe/$SiO_2$ core-shell nanoflakes, respectively. XRD patterns of Sample A and Sample B show prominent diffraction peaks associated

with cubic α-Fe. Magnetic hysteresis loops measured at room temperature show that both samples exhibit excellent soft magnetic properties. The saturation magnetization and coercivity of Sample A are 193 emu g-1 and 23 Oe, while those of Sample B are 176 emu g-1 and 23 Oe, respectively, due to the nonmagnetic $SiO_2$ nanoshell causing a decrease in the saturation magnetization of Sample B [68].

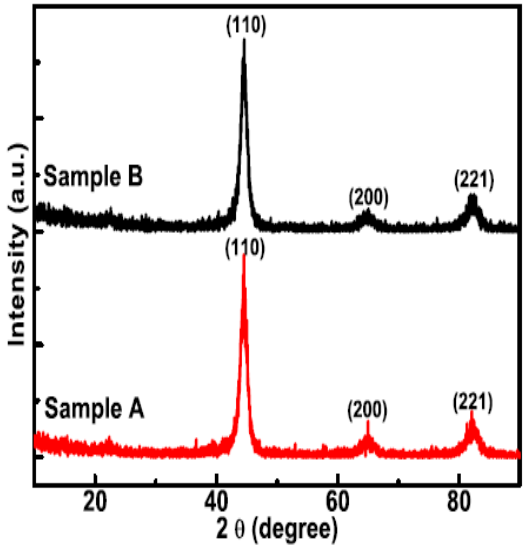


Figure 1.15: The XRD patterns of Sample A and Sample B [68].

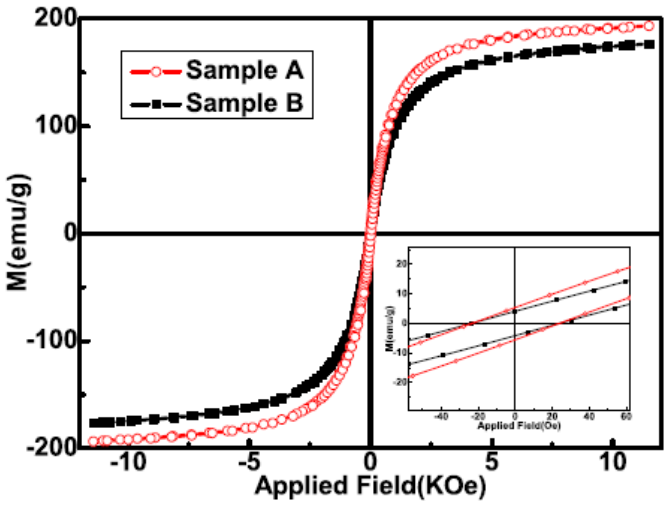


Figure 1.16: The magnetic hysteresis loops of Sample [68].

In 2010, S.F. Lomaeva et al. investigated the structural and phase composition, as well as magnetic properties of Fe-$SiO_2$ nanocomposites produced by high energy ball milling. The Fritsch P_7 planetary ball mill was used with a vessel of 45 $cm^3$ volume and 20 milling balls with a diameter of 10 mm made of ShKh15 strengthened ball-bearing steel (1% C, 1.5% Cr), which minimized powder contamination. The powder mass loaded into

the vessel was 10 g, and Fe-$SiO_2$ composites were produced from Fe and amorphous $SiO_2$ mixed in weight proportions of 30:70 and 70:30. The milling was carried out in the atmosphere of Ar or air for 0.25-64 hours. The Fe-$SiO_2$ system formed isolated particles ranging in size from 2 to 20 nm with a complex phase composition (Fe, FeSi alloy, FeO, $FeSiO_3$), and the quantitative ratio of these phases depended on the milling media. The magnetic properties of the systems obtained were determined by the initial mixture's composition and mechanical alloying conditions. The coercive force was not significantly influenced by the sizes of Fe particles or the presence of FeO and $FeSiO_3$, but rather by oxygen in Fe particles in the form of a solid solution. The heating of the vessel's outer wall during mechanical treatment did not exceed 80°C due to forced air cooling [69].

Tahir Ahmad et al successfully synthesized silica sand nanoparticles using zirconia beads as grinding media in 2012. The nanoparticles were characterized using Zetasizer nanoparticles analyzer and FESEM analysis, and the average particle size was found to be 54.18 nm. The addition of these silica sand nanoparticles as reinforcement to iron resulted in a decrease in green density but an improvement in sintered density at 1100$^o$C due to the occurrence of liquid phase sintering mechanism. The microhardness of Fe-$SiO_2$ nanoparticles increased up to 168HV with 20wt.% and sintering temperature of 1100$^o$C. This was confirmed by measuring the diagonal length of the indentation using FESEM analysis, which showed that the Fe-rich phase had more diagonal length compared to the Si-rich phase. The diffusion of silica sand nanoparticles into the porous sites of composites resulted in the formation of FeSi phase, which is the main contributor to the improvement of microhardness [70].

In 2014, G. Pozo López and colleagues reported their findings on a new method for producing iron/iron oxide/$SiO_2$ composites. This technique involved dry milling analytical grade α-Fe (99.4% purity) and $SiO_2$ (99% purity) crystalline powders in a medium energy planetary mill for extended periods of time under air atmosphere. The Fritsch Pulverisette 5 planetary ball-mill with hardened steel balls and vials was used for milling. The precursor powders were first milled separately to reduce their particle size until both had a similar mean crystallite size, approximately 65 nm for α-Fe and 50 nm for quartz. The pre-milled powders were then mixed in a proportion of 50 wt.% α-Fe and 50 wt.% $SiO_2$, and the mixture was milled at a speed of 200 rpm with an initial ball-to-powder mass ratio of 10:1. The milling time varied from 0 to 340 h in dry air atmosphere without any additive.

The XRD patterns of the powders after different milling times were presented in Figure I.15 [71].

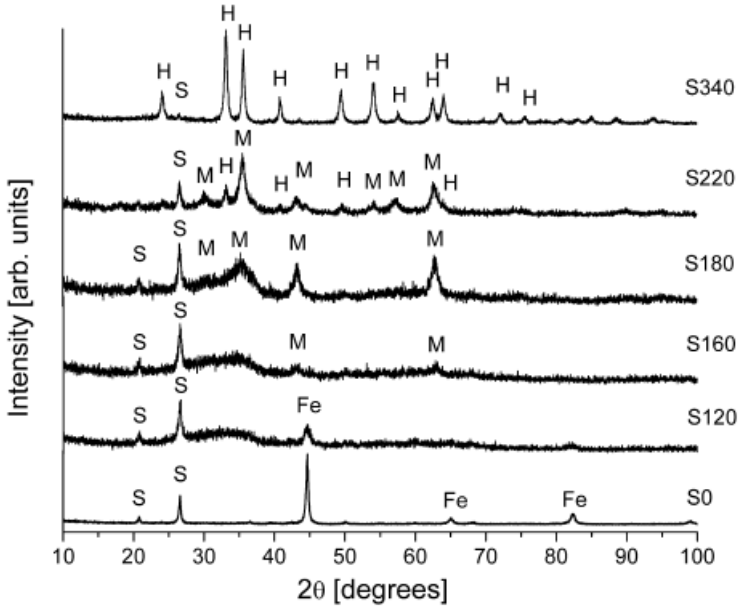


Figure 1.17: X-ray diffraction patterns of samples Sx after different milling times [71].

The iron particles examined in this study exhibit ferromagnetic behavior within the temperature range tested, and their magnetization reversal occurs through a coherent rotation mechanism. The significant effective magnetic anisotropy observed is attributed to surface effects. Following grinding for a duration between 160 and 220 hours, the sample consists of superparamagnetic maghemite nanoparticles (8–13 nm) dispersed in amorphous silica. After milling beyond 220 hours, hematite phase emerges and gradually replaces the maghemite nanoparticles. The ferromagnetic contribution to the observed hysteresis loop is likely attributed to hematite particles (about 20 nm) while the remaining maghemite particles may contribute to the superparamagnetic component. Following 340 hours of milling, the sample predominantly comprises of hematite particles embedded in amorphous silica [71].

In 2022 Tetiana Rudeichuk et al prepared three types of compacted (ring form) samples of iron SMCs (S1, S2, S3). We have used Alfa Aesar high-purity iron granules (99.98%, granule size 1-2 mm). As it is shown in the table [72] :

Tableau 1.4: The conditions of mechanical milling for powdered SMCs of Fe.

| The name of sample | The time of milling (min) | The rate of milling (rpm) | BRP |
|---|---|---|---|
| **S1** | 120 | 500 | 3 : 1 |
| **S2** | 120 | 500 | 6 : 1 |
| **S3** | 120 | 500 | 9 : 1 |

To achieve the necessary physical and magnetic properties, it is crucial to investigate magnetization processes, determine the appropriate chemical composition of the material, establish the correct procedure for preparing powder materials suitable for compaction, select the appropriate type of alloy as a milling precursor (such as BPR), and understand the morphology of particles and compaction properties. Increasing the ball to powder ratio results in a decrease in coercivity value. The reduction in coercivity with increasing BPR for compacts can be attributed to the following: a higher BPR leads to smaller mean particle size, resulting in less deformation during compaction and a lower probability of creating structural defects for domain wall displacement [72].

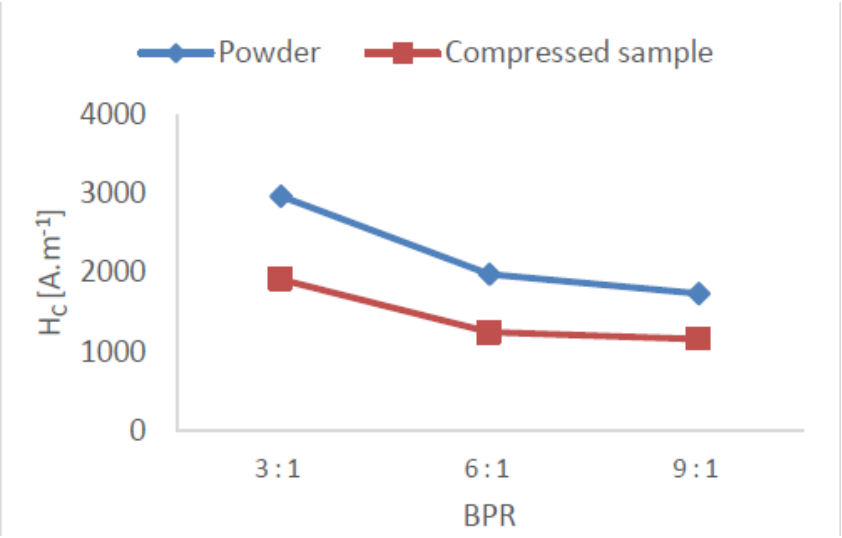


Figure 1.18: The values of the coercivity of powder and compacted SMCs of Fe [72].

Developing new magnetic materials for energy saving is a major goal. Soft magnetic composites (SMCs) are a potential solution for energy production and transformation. Sviatoslav Vovk et al in 2023 synthesized high purity iron powder samples (99.9%) from

Alfa Aesar with particle sizes between 1 and 2 mm. The powder was milled and sieved to obtain particles between 125 μm and 200 μm. The iron powder was then coated with a layer of $SiO_2$ using the Stöber method, resulting in a $SiO_2$ content of 2.57 wt%. The content of ferrite was found to significantly modulate the magnetic properties of the Fe/$SiO_2$/ferrite SMCs. Choosing a ferrite with a sufficiently high Curie temperature was shown to be important for the permeability spectra behaviour of the hybrid composites as a function of temperature. The Fe/ferrite SMCs exhibited a magnetisation reversal phenomenon that was partially reduced by increasing temperature. The lowest excess loss as a function of temperature was observed at higher frequencies associated with more efficient domain wall movement. The Fe/$SiO_2$/2 vol% ferrite composite achieved an initial permeability of 84 with good frequency stability and energy loss of 57 J/$m^3$ at 0.1 T and 35 kHz. Ferrite as an insulating layer in SMCs has the potential to meet high-frequency requirements while maintaining energy efficiency [73].

# CHAPTER 2

## Elaboration and characterizations techniques

# 2. Experimental techniques :

## 2.1 Introduction :

This chapter details the experimental methodology employed and is divided into two parts. The first part focuses on our nanocomposites, while the second part deals with the techniques used for characterization. The $Fe/SiO_2$ alloy was produced via mechanosynthesis using a PM 400 mill with varying milling times. X-ray diffraction was used to examine the kinetics of alloy formation and the evolution of structural parameters during milling. Additionally, vibrating sample magnetometer (VSM) and a Foucault current analyzer were employed to investigate changes in magnetic and electromagnetic properties, respectively.

## 2.2 Overview of iron and silica properties :

### 2.2.1 Iron (Fe) :

Iron has been known to humans since ancient times, it has been widely used as a raw material since the Iron Age (1200 BC), mainly in the production of steel. Fe is one of the most abundant elements on terrestrial planets, accounting for approximately 30wt% of the Earth, Venus, and Mars. It has three valence states: $Fe^0$, $Fe^{+2}$, and $Fe^{+3}$, each with a specific electronic configuration [74].

Tableau 2.1: Electonic configuration of iron three states [74].

| State | Electronic configuration |
|---|---|
| **$Fe^0$** | Ar, 3d6, 4s2 |
| **$Fe^{+2}$** | Ar, 3d6 |
| **$Fe^{+3}$** | Ar, 3d5 |

The versatility of iron stems from its magnetic properties, making it a significant material. At atmospheric pressure, iron exhibits two distinct crystal structures: body centered cubic (bcc) and face-centered cubic (fcc) [75].

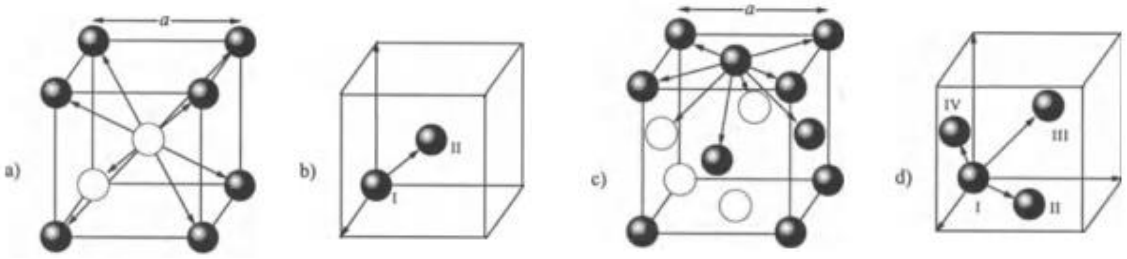


Figure 2.1: a) bcc lattice, b) unit cell of bcc lattice, c) fcc lattice and d) unit cell of fcc lattice [75].

### 2.2.2 Silica ($SiO_2$) :

Silicon dioxide, also known as silica, is a major component of rock-forming minerals in magmatic and metamorphic rocks, as well as sediments and soils. Quartz, which makes up 12-14 wt% of the lithosphere, is the most common form of free silica [76].

Silicon dioxide exists in various allotropic forms such as quartz, cristobalite, tridymite, coesite, stishovite, and vitreous silica These forms, with the exception of stishovite, are composed of the same basic structural unit, the $SiO_4$ tetrahedron [77]. The figure below shows the structure of silica.

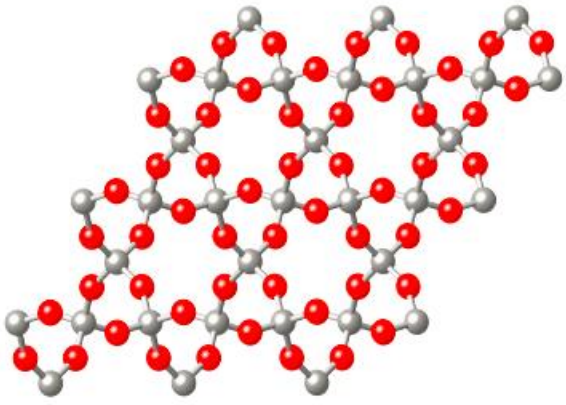

Figure 2.2: Representation of the silica lattice, oxygen atoms in red and silicon atoms in gray [78].

Nanosilica has garnered considerable research interest due to its importance in various industrial applications. Studies have shown that silica is a material with controllable morphology that can be modified with various structures to achieve specific properties. Moreover, a combination of silica with magnetic, catalytic, bioactive, or

photoactive materials such as iron, nickel, and cobalt in oxide forms and/or their combinations enables the extensive design and functionalization of silica-based materials[79].

Metal-SiO2 nanocomposites have gained significant interest due to their magnetic, electric, and catalytic properties [80].

## 2.3 Elaboration technique :

### 2.3.1 Conditions of elaboration :

The $Fe/SiO_2$ nanocomposite was synthesized using a PM 400 planetary ball mill (Figure II.4 ) , which was equipped with two tungsten carbide pots. The milling process involved a 15-minute cycle at 250 rpm, followed by a 15-minute break to prevent a significant increase in temperature inside the jars. Each test sample was prepared by adding 10 g of the elemental powder mixture to the pots with WC balls at a mass ratio of 1:10. The raw materials utilized in this study had a mean particle size and purity of 60 µm and 99.5% for Fe, and 40 µm and 99% for $SiO_2$, respectively.

Figure 2.3: PM 400 planetary ball mill [81].

### 2.3.2 Operating Principle :

The grinding jars are arranged eccentrically on the sun wheel of the planetary ball mill. The rotational movement of the sun wheel is in the opposite direction to the rotation of the grinding jars, in a ratio of 1: -2 (or 1: -2.5 or 1: -3).

The grinding balls in the grinding jar are influenced by superimposed rotational movements, called Coriolis forces. The differences in speed between the balls and the grinding jar result in an interaction between the forces of friction and impact, which releases high dynamic energies.

The interaction of these forces allows for a highly efficient degree of grinding in planetary ball mills [81].

## 2.4 Characterization Techniques :

Advanced techniques and skills are necessary for the development of nanomaterials, in order to achieve higher quality images, comprehend nanostructures, and enhance synthesis strategies [82]. we are intrested in the following methodes :

### 2.4.1 Scanning Electron Microscope (SEM) :

The SEM is a multifunctional and sophisticated instrument that is widely used to investigate surface phenomena in materials. Samples are exposed to high-energy electrons in the SEM, and the resulting electrons and X-rays are analyzed to provide information about the material's topography, morphology, composition, grain orientation, and crystallographic properties. Morphology refers to the shape and size of a material, while topography refers to its surface characteristics (texture, smoothness, or roughness) [83].

The SEM machine comprises of several components including [84]:

a) An electron gun that produces high-energy electrons.

b) A column to guide the electrons through one or more electromagnetic lenses.

c) A deflection system with scan coils.

d) An electron detector to capture backscattered and secondary electrons.

e) A chamber for the sample.

f) A computer system with a viewing screen to display the scanned images and a keyboard to control the electron beam.

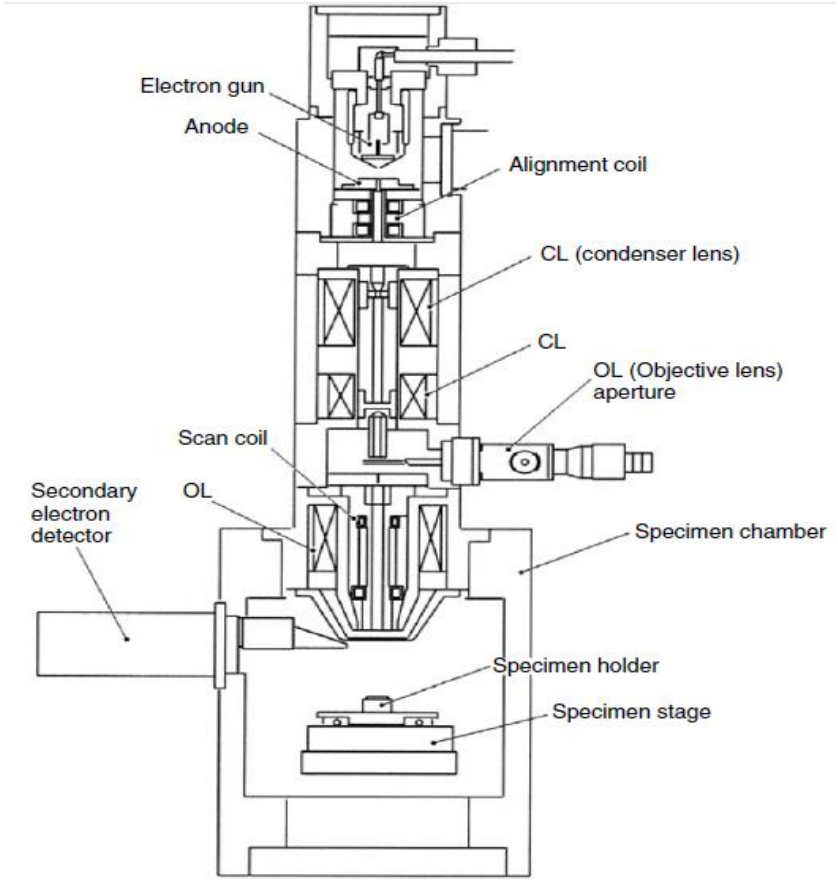


Figure 2.4: Schematic diagram of a scanning electron microscope (JSM 5410, courtesy of JEOL, USA) [85].

A scanning electron microscope (SEM) forms images through a shower of high-energy electrons produced by either thermionic or field emission mechanisms. Primary electrons collide with the valence electrons of atoms on the sample's surface, producing secondary electrons. Electromagnetic lenses guide the electron shower to the sample surface, and a scanning coil controls the electron spot size. A secondary electron detector collects the secondary electrons for image formation, while backscattered electrons are collected to produce an image with differential contrast between regions of high and low atomic number elements. X-ray signals produced can also be utilized for chemical identification of materials on the surface of atoms [86].

In SEM, energy dispersive spectroscopy (EDS) is used for elemental analysis of surfaces by measuring the energy and intensity distribution of X-ray signals produced when the electron beam strikes the specimen's surface. This technique allows for precise determination of the elemental composition at a point, along a line, or in a defined area. Elemental maps are used to locate areas with high concentrations of elements present at greater than 1% by weight. However, as the electrons penetrate only 0.02-1.0 mm into the sample, appropriate sample preparation is necessary for information about the bulk. EDS is commonly used for metallic and ceramic specimens and their weathering crusts or corrosion products [87].

**2.4.1.1 Equipment :**

The morphological changes for various milling durations and aspects of the creation of the nanocrystalline were examined using a scanning electron microscope (Gemini SEM 300) with 30 kV acceleration voltage. The instrument was also equipped with an X-ray dispersive energy spectrometer (EDS). The analyzed samples (powders) were deposited on conductive aluminum supports.

Figure 2.5: Equipment of the SEM apparatus equipped with an EDS analyzer.(CRTI)

### 2.4.2 X-Ray Diffraction (XRD) :

XRD is a technique used for the analysis of single crystal or polycrystalline materials. Its primary use is for identifying and characterizing compounds based on their diffraction patterns. The majority of XRDs operate using reflection geometry, with the X-ray source and detector located on the same side of the sample. The scattered X-rays from the source pass through the sample and onto the detector, where they constructively interfere with each other. The Bragg–Brentano (parafocusing) Law is used to determine various characteristics of the materials based on this interference. The measurements are made in Angstroms, where 1 Angstrom is equal to 0.1 nm. This instrument typically includes a source, primary optics, sample stage, secondary optics, and a detector [88].

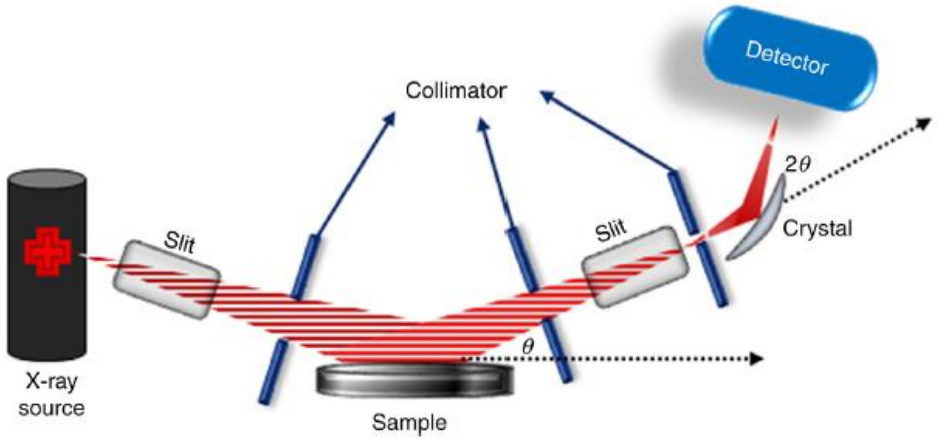


Figure 2.6: Illustration of X-ray diffraction (XRD) [88].

#### 2.4.2.1 Bragg's law :

Bragg's law is the basis of X-ray diffraction and provides a relationship between the position of a peak in a diffraction pattern and the spacing between planes of atoms in a material. When X-rays with wavelengths comparable to atomic spacings interact with a crystalline material that has an ordered arrangement of atoms in three dimensions, the periodic repetition of the planes of atoms leads to the constructive and destructive interference of X-rays, resulting in diffraction patterns. The constructive interference produces diffraction peaks that satisfy Bragg's law [89].

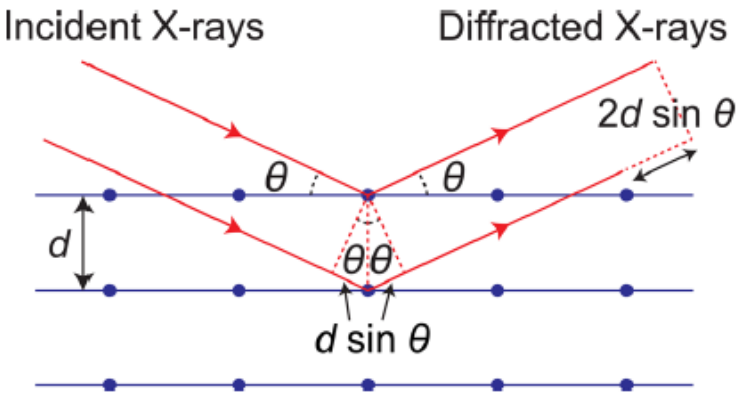


Figure 2.7: Schematic diagram showing the Bragg diffraction of x rays from atomic planes of the crystalline material with the interplanar distance of d [89].

$$n\lambda = 2d \sin\theta \qquad (2.1)$$

The distance between atomic planes (d), the angle of the incident X-rays with respect to the atomic plane (θ), the order of reflection (n), and the X-ray wavelength (λ). When the phase shift between X-ray waves is equal to an integer multiple of the wavelength, the Bragg condition for diffraction is fulfilled and diffracted X-rays undergo constructive interference. This results in diffraction peaks which can be used to identify and characterize the material. XRD patterns are typically collected by recording the intensity of diffracted X-rays as a function of 2θ [89].

### 2.4.2.2 diffractometers in laboratory equipment :

A goniometer is a key component of diffractometers found in laboratory equipment. It allows for precise movement of the X-ray source, sample, and detector in relation to each other. Bragg-Brentano geometry is commonly used, and the reflection mode is preferred for investigating powder or massive samples due to strong X-ray beam absorption. There are two main types of goniometers: θ/θ where the sample is fixed ( Fig 2.8.a) and θ/2θ for which the X-ray source is at a fixed position while the sample and the detector are moving ( Fig 2.8.b) [90].

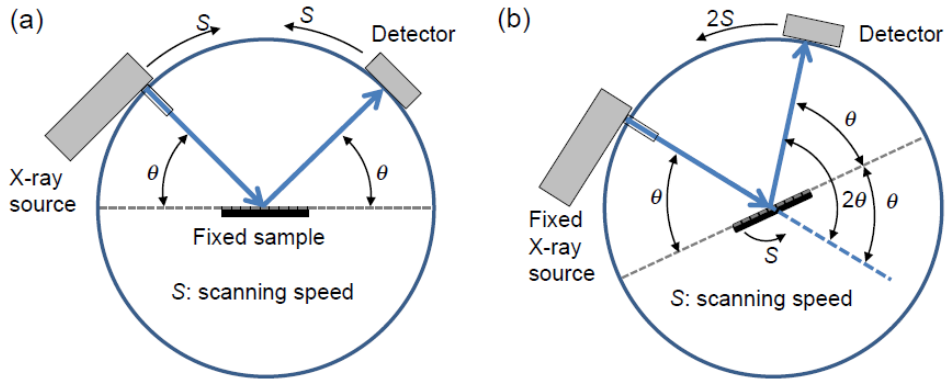


Figure 2.8: Principle of (a) θ/θ goniometers and (b) of θ/2θ goniometers [90].

### 2.4.2.3 Equipment :

A Cu Kα radiation XPERT PRO X-ray diffractometer (XRD) was used to analyze the formation kinetics during mechanical milling within the 2θ range of 10° to 100°.

Figure 2.9: XPERT PRO diffractometer of X-Ray diffraction.(CRTI)

### 2.4.3 Vibrating sample magnetometer (VSM) :

The VSM is a coveted scientific instrument capable of measuring magnetic moments up to $10^{-9}$ $Am^{-2}$. It was invented by Simon Foner at Lincoln Laboratory, Massachusetts Institute of Technology (MIT). Faraday's law of induction serves as the foundation for

operating the VSM. This principle dictates that a magnetic flux that varies over time generates an electromotive force (EMF) expressed as:

$$e.m.f. = -\mathrm{N}\frac{d(BA\cos\theta)}{\mathrm{dt}} \qquad (2.2)$$

The equation represents the electromotive force (e.m.f.) induced by a time-varying magnetic flux, as described by Faraday's law of induction. It includes the number of loops N, coil turn area A, and the angle between the magnetic field and the direction normal to the surface, denoted by θ. The negative sign indicates the operation of Lenz's law [91].

An electromagnet is used to generate a uniform magnetic field H in an electromagnet-based VSM. The sample, a magnetic material, is vibrated within this field, inducing an electric current in sensing coils placed in a suitable position. The magnitude of the resulting voltage induced in the sensing coils is directly proportional to the magnetic moment of the sample. Integrated cryostats and furnaces allow for variable temperature measurements to be performed, ranging from <4.2 K to 1273 K [92].

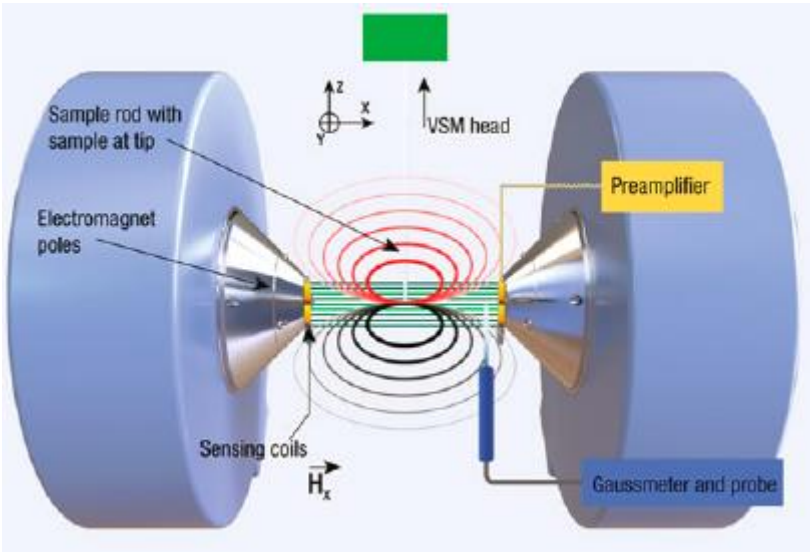


Figure 2.10: Schematic representation of a VSM. The red and black contours represent the dipole magnetic field of a magnetized sample [92].

The VSM sensing coils produce an induced voltage, which can be expressed as:

$$V_{emf} = m\ A\ f\ S \qquad (2.3)$$

Here, m represents the magnetic moment, A is the vibration amplitude, f is the vibration frequency, and S is the sensitivity function of the VSM sensing coils. The sensitivity function S is determined through calibration of the VSM with a magnetic calibrant, which is a material with a known magnetization at a specific applied field H[92].

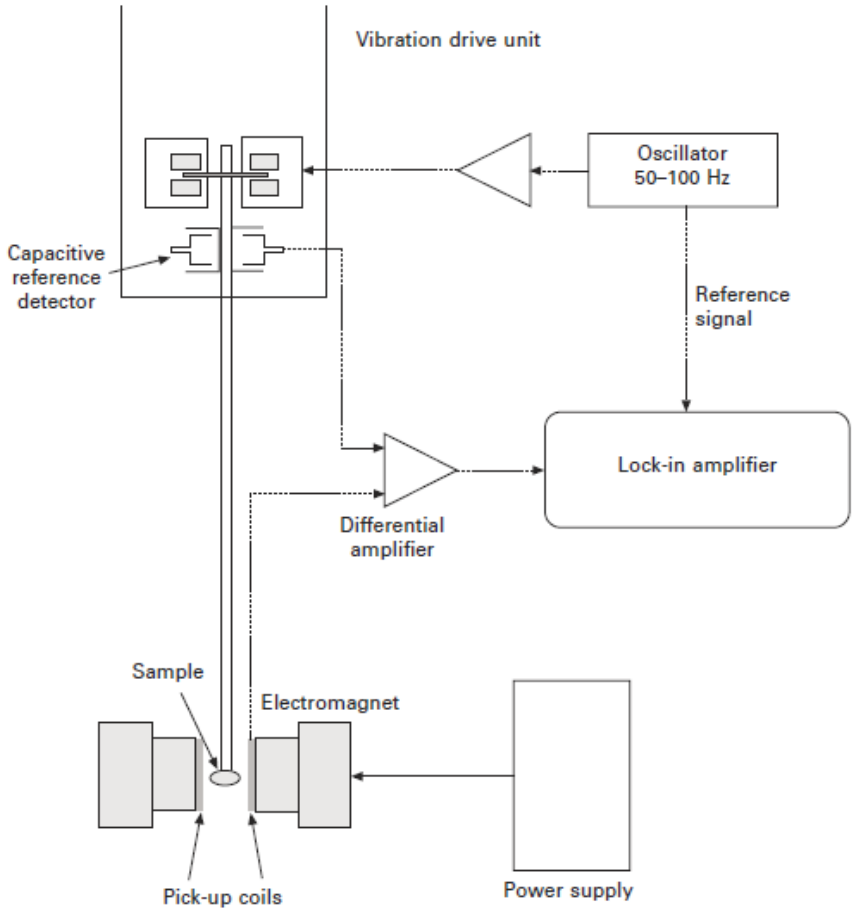


Figure 2.11: Schematic diagram of the essential features of a vibrating sample magnetometer [93].

### 2.4.3.1 Equipment :

The magnetic characteristics were monitored as a function of milling time using a MicroSense EV9 vibrating sample magnetometer.


Figure 2.12: Vibrating sample magnetometer (VSM).(CRTI)

### 2.4.4 Eddy current testing (ECT) :

The fundamental principle of ECT remains unchanged since its inception in 1879, which employs Oersted's law of electromagnetic induction to induce eddy currents in conductive materials. As shown in Figure below, an alternating current flowing through a testing coil generates an alternating magnetic field with flux density B. By increasing the number of windings in the coil, the flux density increases linearly with the current. The total magnetic flux ($\phi_p$) within the coil is the product of B and the coil's area. When the coil is placed on or near a conductive material (specimen), the magnetic field penetrates the material and induces eddy currents with closed circular paths, as per Lenz's law. These eddy currents produce a secondary magnetic field, opposing the primary magnetic field, and inducing magnetic flux ($\phi_s$), which also opposes the primary flux. By Faraday's law, an induced magnetic field cutting across a conductor generates an electrical current in the conductor. Changes in the material's electrical properties, such as conductivity and permeability, affect the induced current in the testing coil, causing a change in the coil's impedance due to mutual inductance. The ECT technique measures the impedance signals sensed by the search coil as an indicator of the specimen's physical properties and defects, utilizing the effects of electromagnetic fields and induction [94].

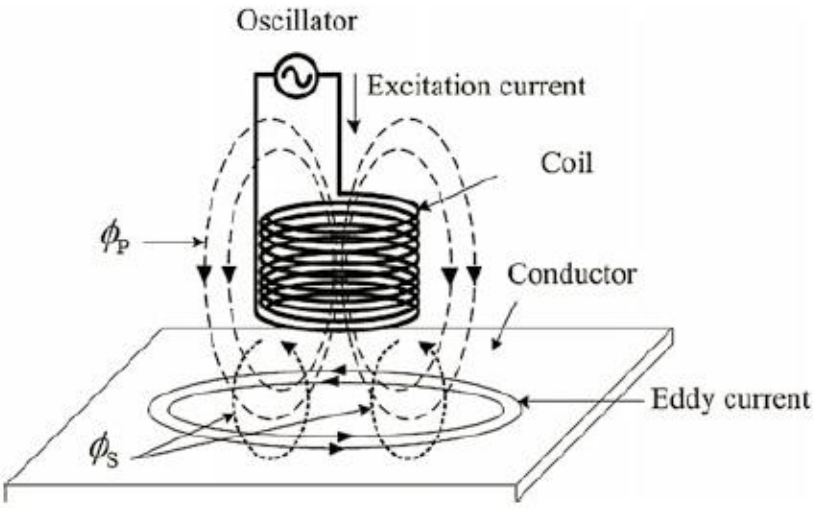


Figure 2.13: Concept diagram of the principle of eddy current testing [94].

**2.4.4.1 depth of penetration :**

In eddy current testing, a crucial aspect to consider is the depth of penetration which is limited due to the skin effect. This phenomenon causes the alternating currents to concentrate near the surface, as the opposing field produced by the eddy currents cancels out the applied magnetic field. The skin depth, which is the depth where the current magnitude reduces by a factor of 1/e, depends on various factors such as the oscillating frequency, the magnetic permeability, and the conductivity of the material. As the frequency increases, the eddy currents become more focused near the surface where the energy flows from the excitation source. The skin depth is mathematically defined as [95]:

$$\delta = \sqrt{\frac{2}{\omega\mu\sigma}} \qquad (2.4)$$

Where :

- δ is skin depth (m)
- σ is electrical conductivity (S/m)
- ω is frequency (Hz)
- μ is magnetic permeability (H/m)

If the thickness of the material under test is less than the proposed 3δ effective penetration depth of the eddy current, it will have a significant impact on the measurement.

### 2.4.4.2 Equipment :

The experimental equipment that we used consists essentially of the following elements :

- An impedance analyzer of Hp brand operating in a frequency range from 20Hz to 1MHz.
- A probe characterized at the CRTI laboratory (consisting of 2000 turns).
- A sine wave generator to excite the sample under control.

Figure 2.14 : Analyseur d'impédance de marque Hp.(CRTI)

# CHAPTER 3

## Results and discussions

# 3. Results and discussions:

## 3.1 Introduction:

This chapter aims to present and interpret the results of the studies conducted on the Fe/SiO2 milled powder under different time periods (0h, 5h, 15h, 30h) with a specific processing cycle of 15 minutes at 250 rpm, followed by a 15-minute break. The raw materials used in this study had a mean particle size and purity of 60 µm and 99.5% for Fe, and 40 µm and 99% for $SiO_2$. The morphology of the powder was analyzed using scanning electron microscopy (SEM) technique, while the microstructure of the alloy was characterized using X-ray diffraction (XRD) technique. Finally, the magnetic properties were determined using a vibrating sample magnetometer (VSM).

## 3.2 Structural characteristics of Fe/ $SiO_2$ :

The X-ray diffraction technique was utilized to study the structural properties of nanocrystalline powder during mechanical milling. The X-ray diffraction (XRD) is employed as the main method for characterizing material properties such as crystal structure, crystallite size, and strain [96]. This approach is widely used to perform quantitative analysis, identify different phases, and analyze structural imperfections. By applying this technique accurately, comprehensive information about the structural characteristics of materials can be obtained [97].

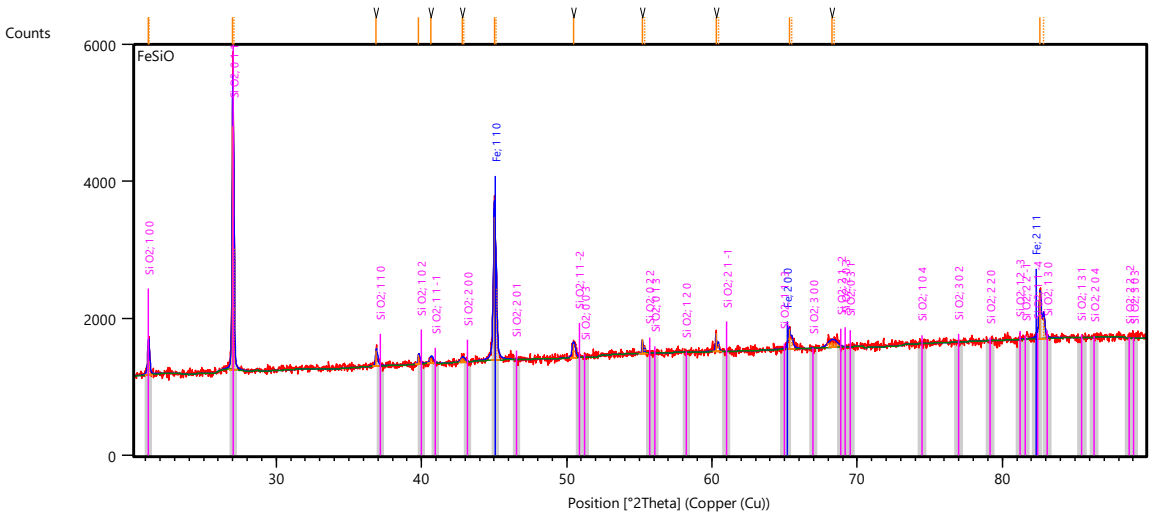

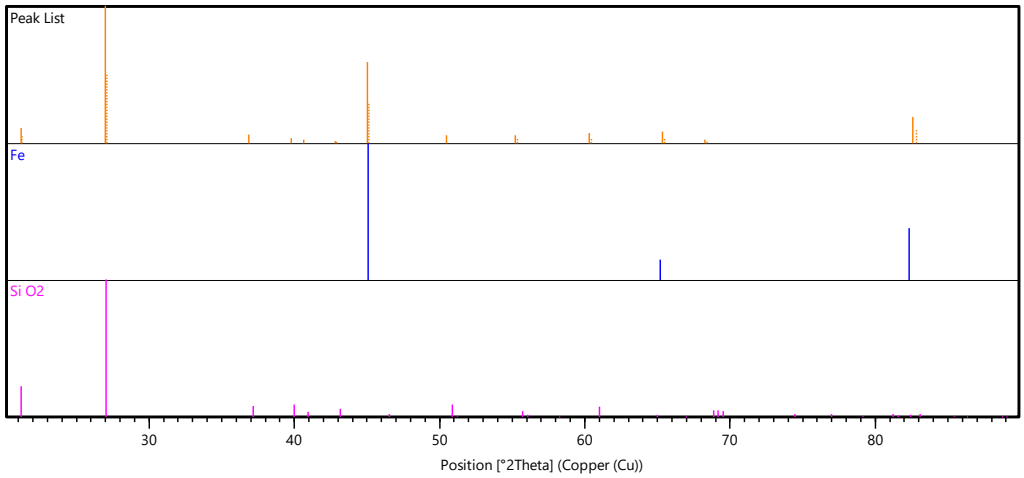


Figure 3.1: XRD-pattern for unmilled Fe/$SiO_2$.

In Figure 3.1, the XRD pattern exhibits clear and well-defined diffraction peaks at specific 2θ angles, indicating the presence of iron and silica peaks. Notably, three distinct peaks corresponding to iron are observed: Fe (1 1 0), Fe (2 0 0), and Fe (2 1 1). These iron peaks are centered around 44.8°, 65.5°, and 82.5°, respectively. Additionally, multiple peaks with varying intensities can be observed, which are associated with the presence of $SiO_2$ in the sample.

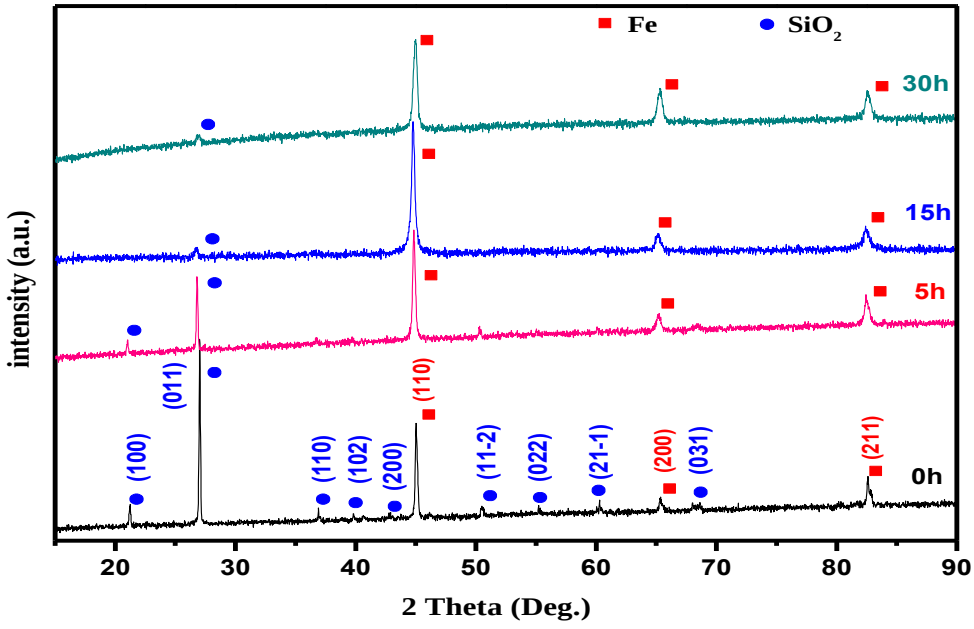


Figure 3.2: XRD spectra at selecting milling times for Fe/$SiO_2$.

In Figure 3.2, the X-ray diffraction (XRD) patterns represent the powders obtained at different milling durations. The red squars present the Fe element while the blue circles refers to the $SiO_2$. After 5 hours of milling, the XRD spectra display three distinct

diffraction peaks corresponding to Fe (1 1 0), Fe (2 0 0), and Fe (2 1 1), along with two prominent peaks attributed to $SiO_2$ (0 1 1) and $SiO_2$ (1 0 0). Following 15 hours of milling, only a single peak associated with $SiO_2$ (0 1 1) is observed, in spite of a reduced intensity compared to earlier. The absence of peaks corresponding to silica indicates the formation of amorphous silica. Alonso-Sanudo et al. [65] declared that a broad halo when visible in the pattern is an indicative of the amorphous nature of the silica.

With the increase in milling time, the intensities of the Bragg peaks for the Fe / $SiO_2$ powder decreased. Additionally, the peaks displayed significant broadening with a slight displacement as it is illustrated at Figure 3.3, indicating the introduction of a substantial number of defects through mechanical alloying. The broadening of the experimental reflection lines can be attributed to the small size of the diffracting grains, lattice strain, and instrumental broadening [98].

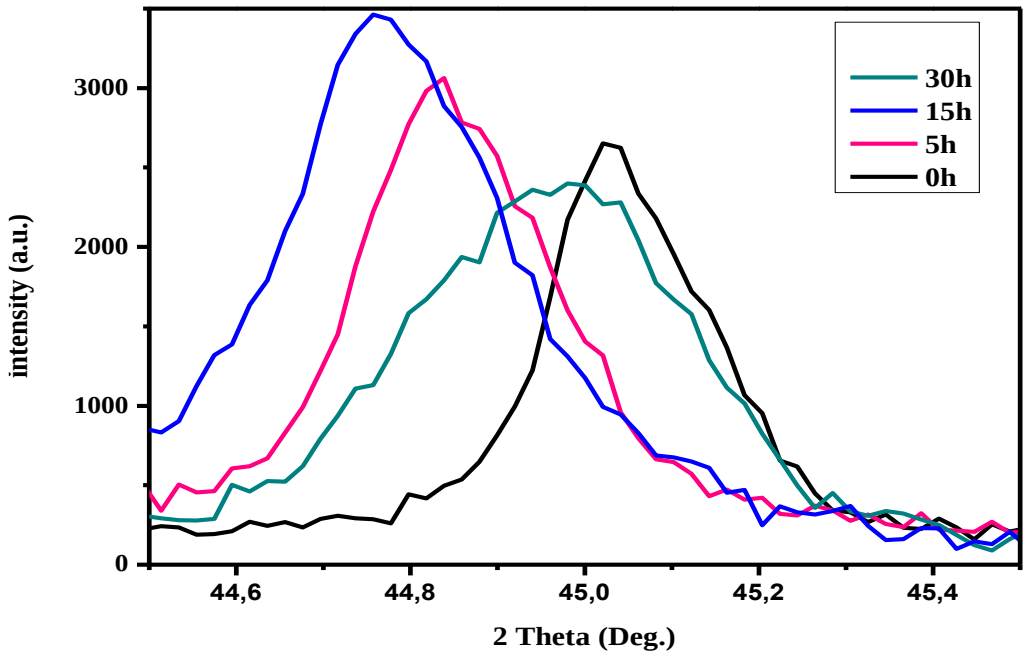


Figure 3.3: XRD pattern showed for 2 Theta [44,5°- 45,5°]

The lattice parameters were calculated for the most intense peak corresponding to the plane (1 1 0) based on the following equation [101]:

$$\frac{1}{d^2} = \frac{h^2+k^2+l^2}{a^2} \qquad (3.1)$$

Whith :

* $d_{hkl}$ : interreticular distance.
* a : the lattice parameters.

* (h k l) : miller indices.

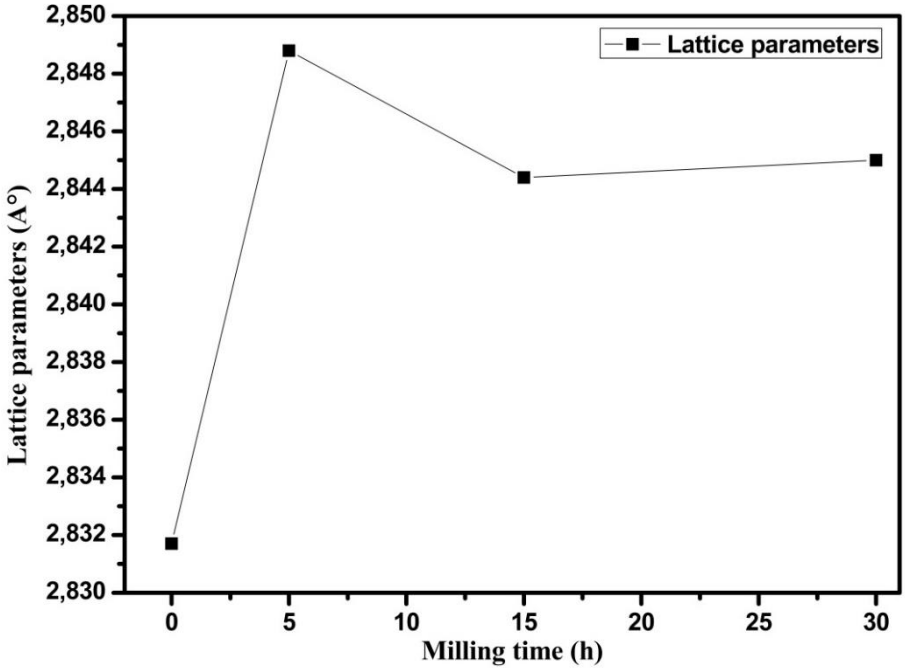


Figure 3.4: Lattice parameters variation for different milling times.

Figure 3.4 illustrates the changes in lattice parameters. These parameters underwent three distinct phases of variation: starting at 0h with a value of 2.8317 A°, reaching a maximum of 2.8488 A° at 5h of milling, slightly decreasing from 5h to 15h to a value of 2.8444 A°, and then reaches a stable state specifically a= 2.8313 A°. Lomayeva et al. [99] determined that the increase in lattice parameter observed during milling is attributed to the presence of an oxide film on the surface of the initial powder, as well as on the walls of the milling vial and the milling balls. As Gayatri Koyar Rane et al. [100] Found that Expansion and contraction of the lattice can appear upon decreasing crystallite/grain size, which leads to variation of lattice parameters.

The crystallite size (D) was determined by applying the Scherrer equation, which utilizes the full-width at half maximum (FWHM) of the diffraction peaks [101] :

$$D = \frac{0.9\lambda}{\beta \cos\theta} \qquad (3.2)$$

The average lattice strain ($\varepsilon$) was calculated using the Stokes and Wilson relation, based on the measurements of the integral breadth of the reflection lines [101]:

$$\boldsymbol{\varepsilon = \frac{\beta}{4\tan\theta}} \qquad (3.3)$$

With:

- λ : X-ray wavelength equals to 1.54059 A°.
- β : full-width at half maximum (FWHM).
- θ : Bragg angle.

The Figure 3.5 showcases the evolution of the crystallite size and lattice strain with the milling time.

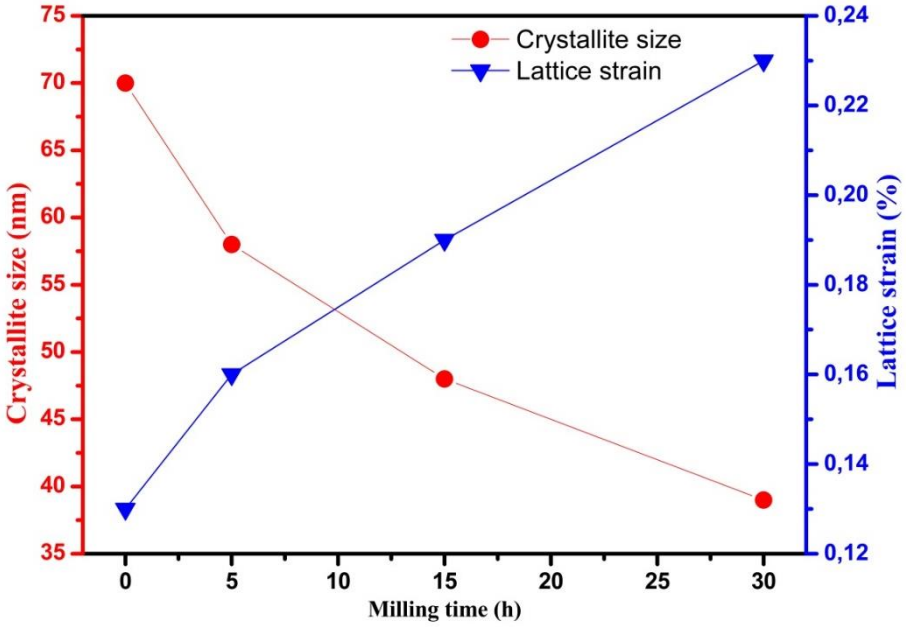


Figure 3.5: the evolution of the crystallite size and lattice strain with the milling time.

An inverse relationship between the crystallite size and lattice strain was witnessed. The crystallite size (D) was observed to gradually decrease from 70 to 39 nm with increasing milling time, while the lattice strain (ε) exhibited a continuous increase from 0.13% to 0.16 % in 5h to reach 0.23% after 30h of milling.

According to B.F. Zou et al. [102], Ball milling not only reduces the size of powders but also decreases the crystallite/ grain size. Smaller grain sizes correspond to larger micro-strains. After ball milling, the grain size decreases and micro-strain increases. This can be attributed to the localized plastic deformation in the form of shear bands, which contain a high density of dislocations that lead to the formation of cells and sub-grains through self-annihilation.

## 3.3 Morphology of $Fe/SiO_2$ alloy:

The milled powder was examined for surface morphology using a Scanning Electron Microscope (SEM), and elemental analysis was performed using energy-dispersive X-ray spectrometry (EDS) as shown in the following Figures:

(a)

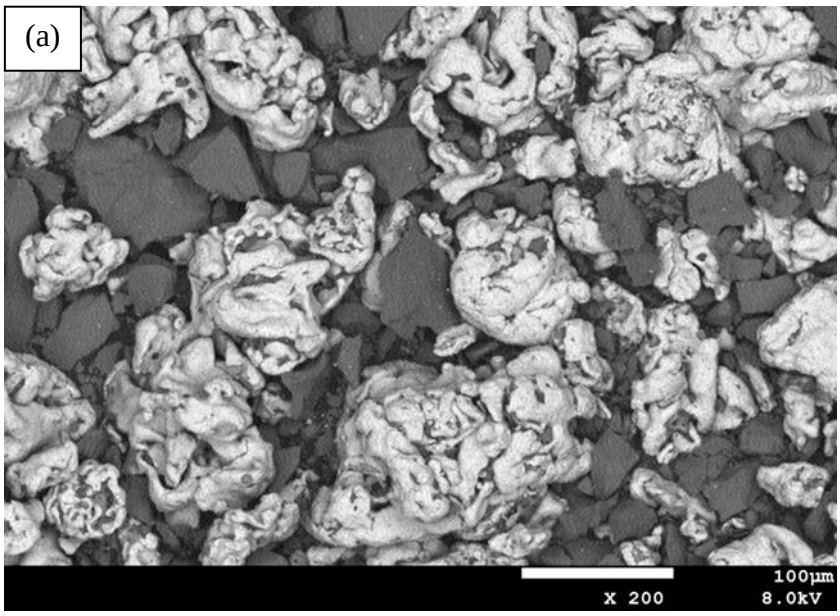


(b)

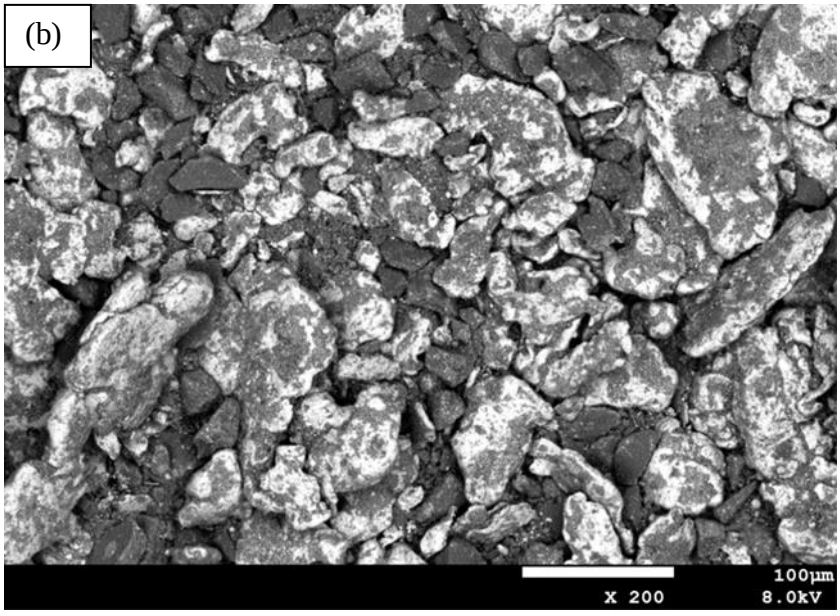

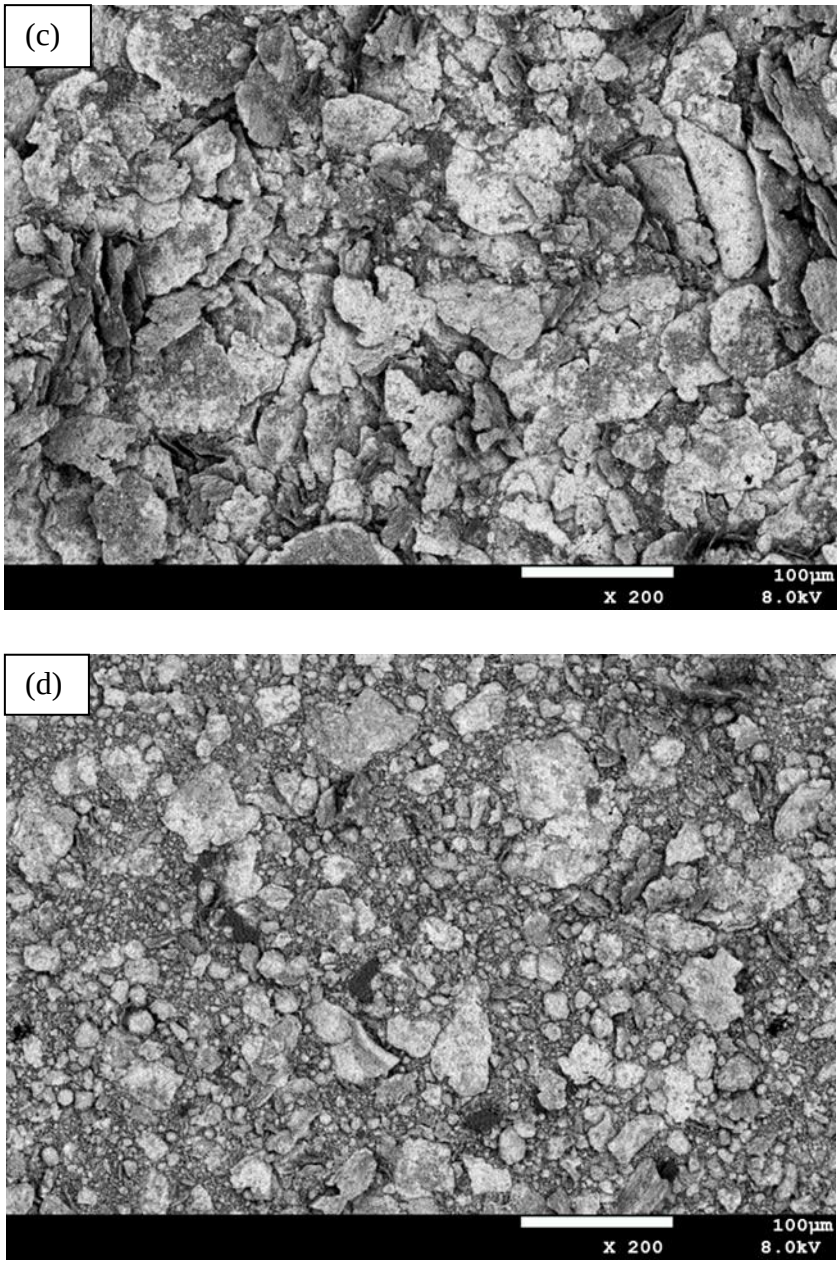


Figure 3.6: SEM images for (a) unmilled $Fe/SiO_2$ and milled $Fe/SiO_2$ for various milling times: (b) 5h (c) 15h (d) 30h.

The SEM micrographs show the actual morphology of Fe and Fe/silica nanocomposite with scale bar of 100µm. Unmilled iron particles exhibit random shape with a dark shade of gray color and have a relatively wide range of sizes, while the silica particles were presented in light irregular to spherical large shapes. Figures 3.5 (b), (c), and (d) illustrate the morphology of the alloy particles after milling for 5 to 30 hours, respectively. After 5 hours of milling, the particles exhibited a mixing effect and began to decrease in size. Subsequently, at the 15-hour mark, a more significant reduction in size was observed, accompanied by noticeable changes in their shape. The images clearly

demonstrate that the milling process causes a transition in the particle size and shape from irregular and spherical to flake-like [103].

After milling Fe/$SiO_2$ mixtures for 30 hours, it can be observed that the resulting products consist of dispersed Fe nanoparticles embedded in the $SiO_2$ matrix. These Fe nanoparticles exhibit irregular shapes.

The EDS analysis is presented in the Figure 3.7 for unmilled Fe/$SiO_2$ mixture as well as the milled mixture for (5h, 15h and 30h).

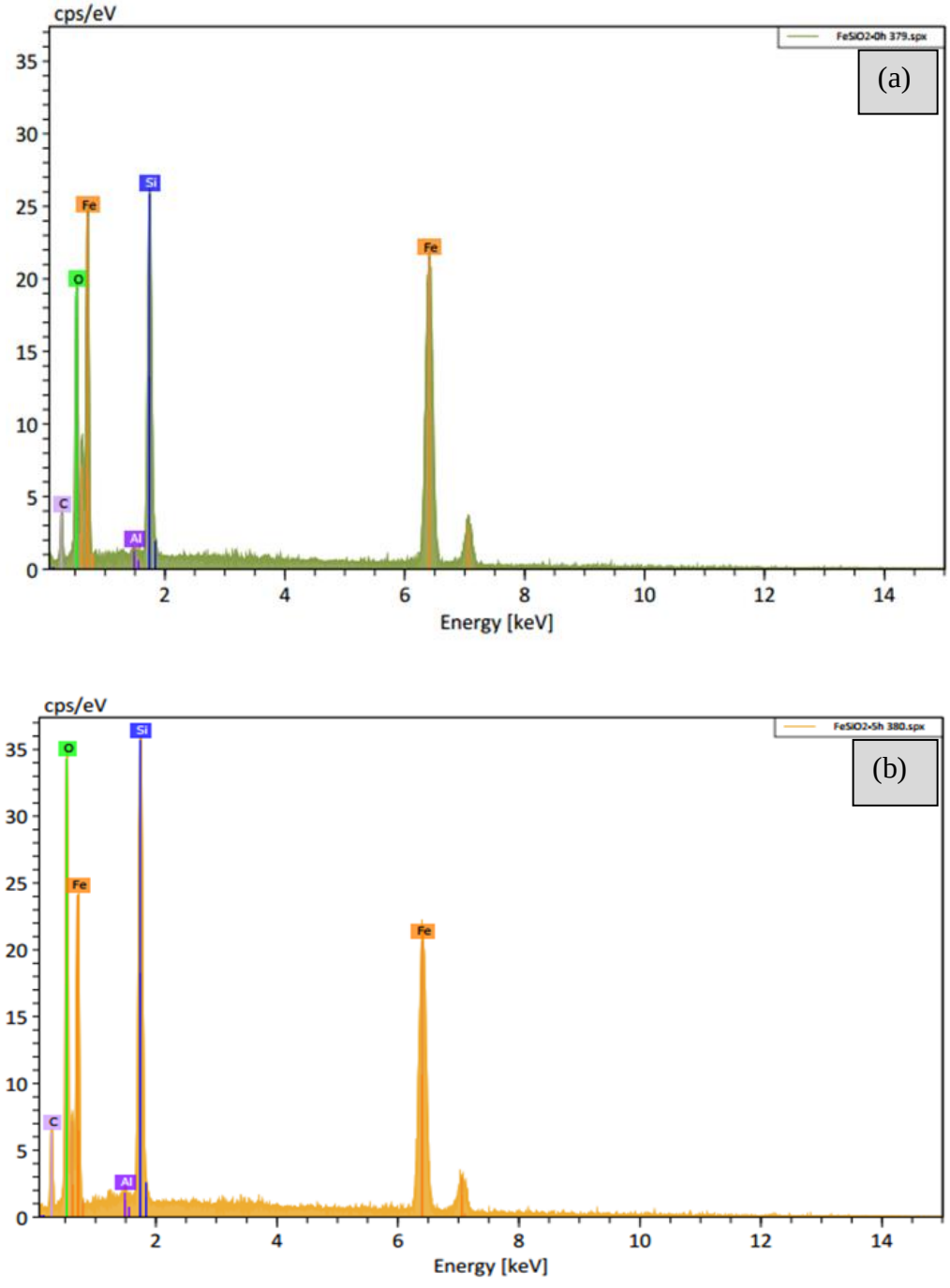

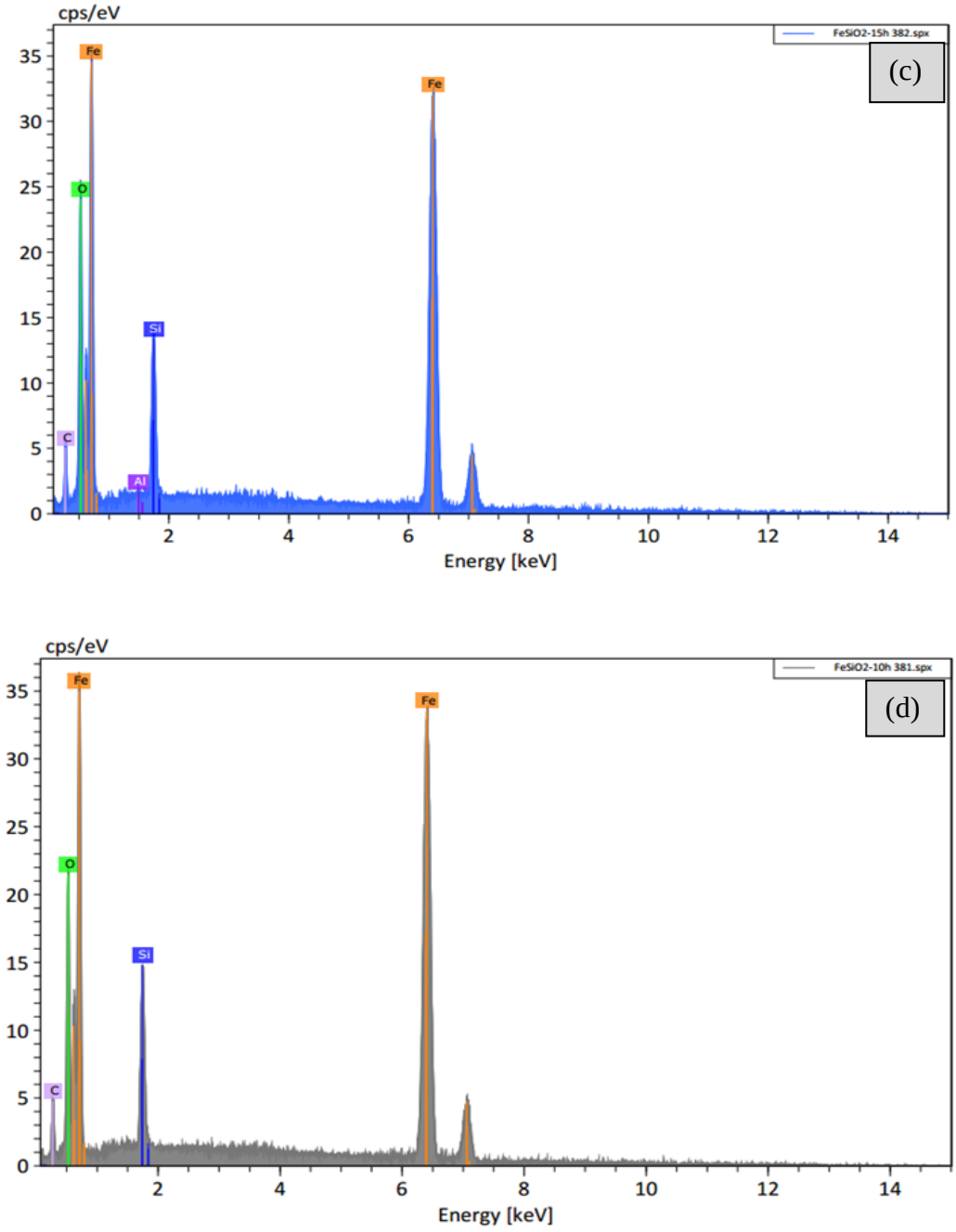


Figure 3.7: EDS spectrum for (a) unmilled $Fe/SiO_2$ and milled $Fe/SiO_2$ for various milling times: (b) 5h (c) 15h (d) 30h.

The results obtained from EDS spectral analysis confirm the presence of both Fe and $SiO_2$ elements in the initial mixture, while indicating the absence of any impurities or contaminants related to the initial materials used in the synthesis, foreign elements introduced during the milling process, or environmental factors.

## 3.4 Magnetic characterization:

The magnetic characteristics of the $Fe/SiO_2$ samples were assessed at ambient temperature employing a vibrating sample magnetometer (VSM). The magnetic hysteresis loops were measured to record the variations in saturation magnetization (Ms), remanence (Mr), and coercivity (Hc) of the milled mixture over different milling durations of 5, 15, and 30 hours.

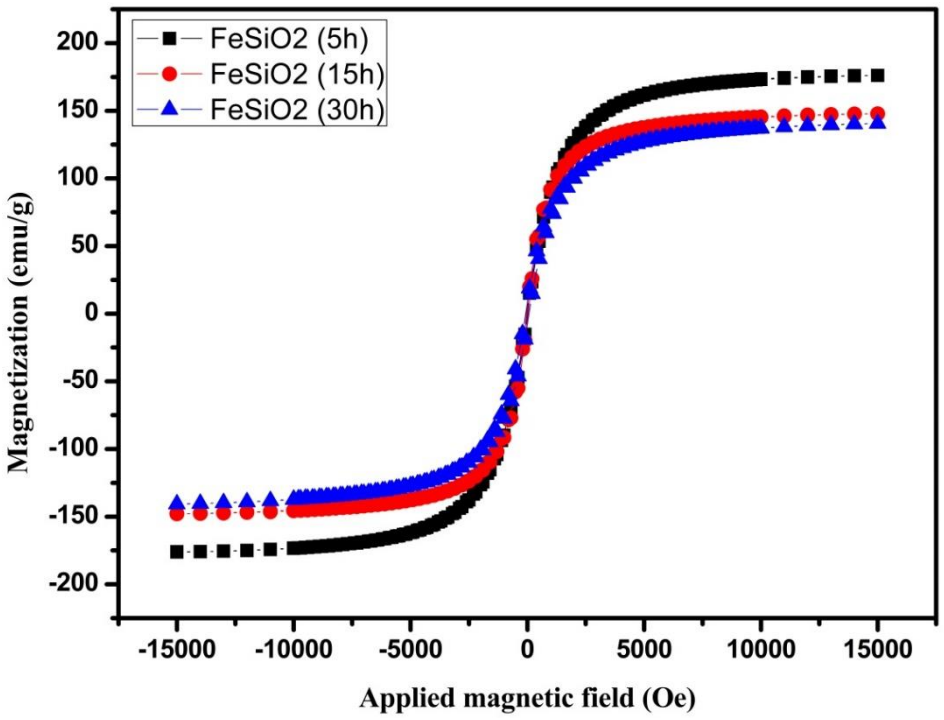


Figure 3.8: Hysteresis loops of nanostructured $Fe/SiO_2$ milled at different times.

Figure 3.8 illustrates the hysteresis loops of the $Fe/SiO_2$ powder at room temperature for various milling durations, measured using a vibrating sample magnetometer (VSM) within a magnetic field range of -15 KOe to 15 KOe. Figure 3.8 shows the ferromagnetic behavior of all samples and the changes of magnetic properties of nanostructured $FeSiO_2$ based on different milling times.it is noticeable the saturation of magnetization at a certain point after amplifying rapidly with the increase in the applied magnetic field.

Figure 3.9 illustrates the evolution of Ms of $Fe/SiO_2$ as a function of milling time. The saturation magnetization (Ms) of the $Fe/SiO_2$ particles was found to be 176.56 emu/g after 5 hours of milling, which gradually decreased to 148.17 emu/g after 15 hours of milling, and further dropped to approximately 140.79 emu/g after 30 hours of milling.

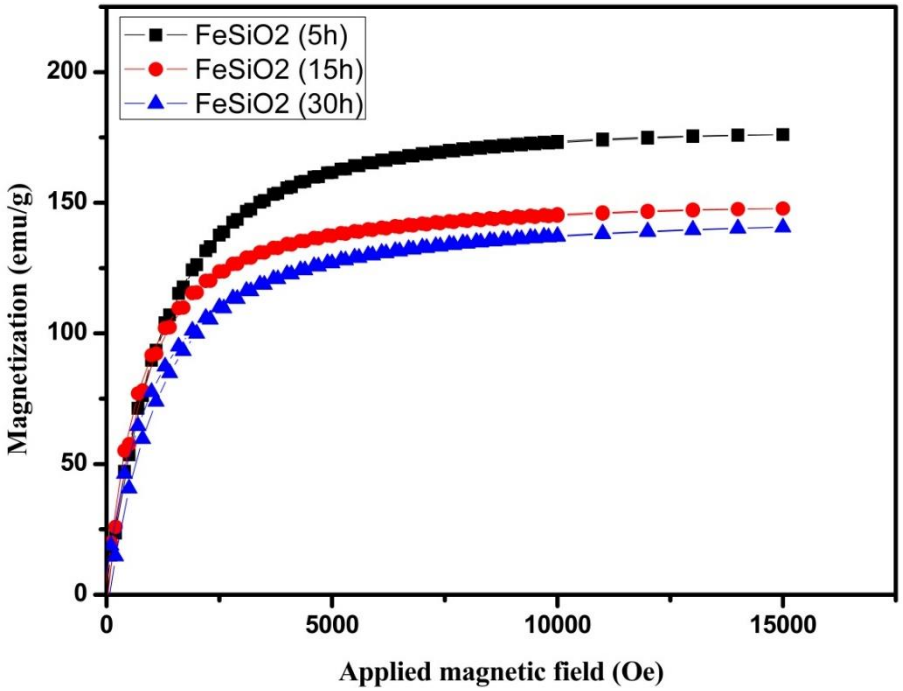


Figure 3.9: the evolution of (Ms) of $Fe/SiO_2$ as a function of milling time.

These values are consistent with the findings reported by E. Thirumal et al. [6] who observed that the high concentration of silica contributes to a reduction in the saturation magnetization. Similar observations were made by Thanh Ho et al. [104], who attributed this phenomenon to the formation of an amorphous silica layer on the surface of the iron core and the influence of small particle size.

The coercivity (Hc) exhibited an increasing trend with milling time. It initially measured 18.14 Oe after 5 hours of milling, increased to 30.54 Oe after 15 hours, and further rise to 69.07 Oe after 30 hours. The enhancement of coercivity shown in Figure 3.10, as suggested by Hang Zhang et al. [105], could be attributed to the exchange anisotropy occurring at the interfaces of Fe nanoparticles (FeNPs) and $SiO_2$. Additionally, Thanh Ho et al. [104] observed that the complete mixing of silica with the iron core did not have a significant impact on the magnetic properties of the iron core.

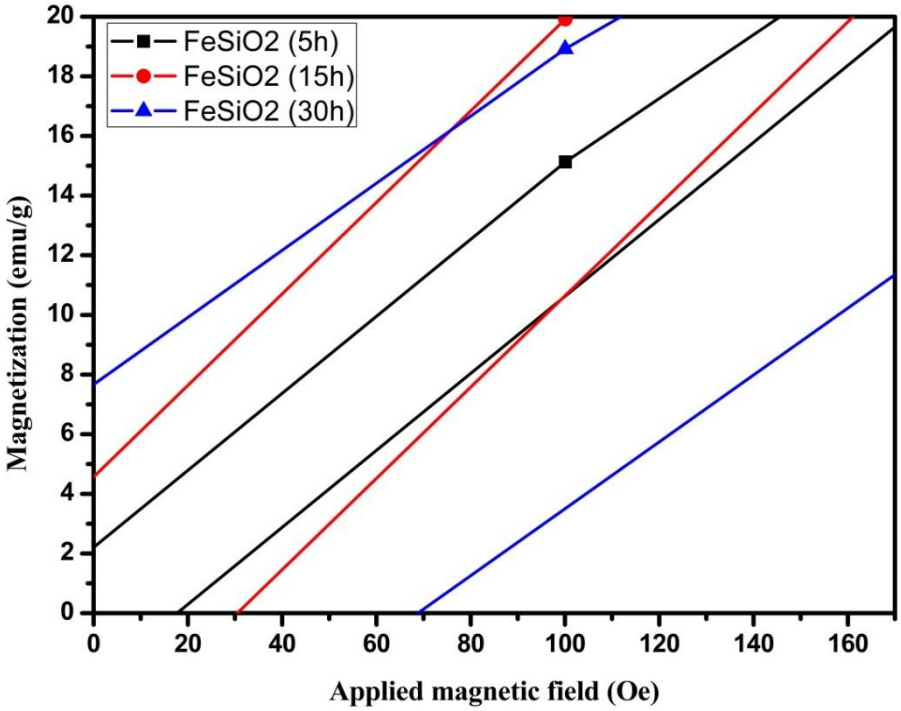


Figure 3.10: the evolution of (Hc) for magnetization equals to zero and (Mr) while Hc = 0 for $Fe/SiO_2$ as a function of milling time.

The remanence (Mr) values exhibited an increase from 2.23 emu/g to 4.58 emu/g and further to 7.73 emu/g after 5, 15, and 30 hours, respectively.

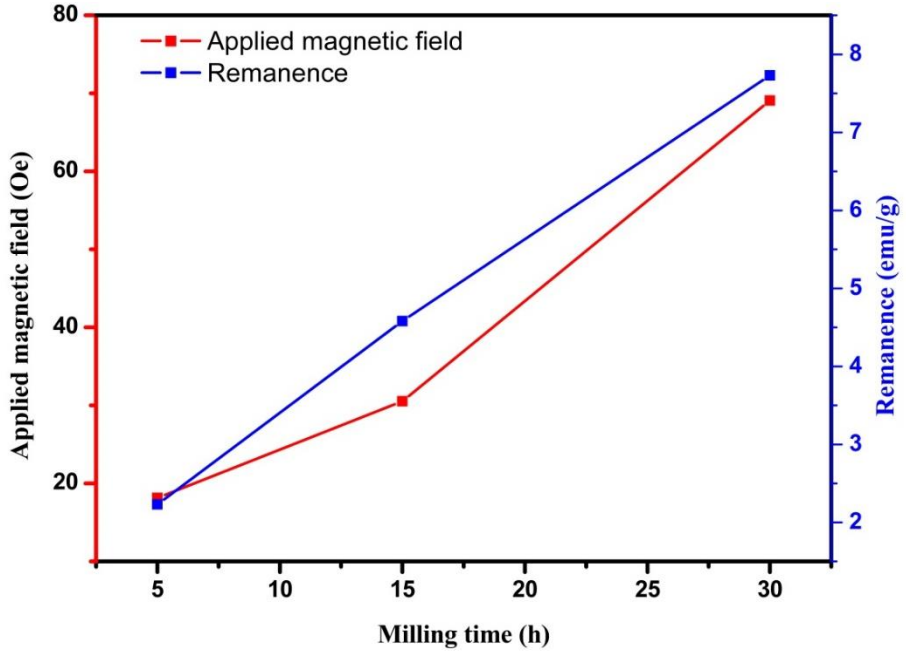


Figure 3.11: the evolution of (Hc) and (Mr) as a function of milling time.

Figure 3.11 demonstrate a positive connection between the coercivity (Hc) and remanence (Mr) values, both show a consistent increase as the milling time progresses.

## Conclusion:

To investigate the structural and magnetic properties of iron-silica nanocomposites, a mechanical alloying approach was employed on Fe and $SiO_2$ samples. The fabrication process involved milling the samples using a PM 400 planetary mill with varying milling times.

X-ray diffraction analysis confirmed the crystalline structure of iron and the amorphous nature of silica after milling. The evaluation of crystallite size and lattice strain revealed a decrease in crystallite size (D) along with the reduction in particle size, reaching 39 nm after 30 hours of milling. Meanwhile, lattice strain (ε) increased, reaching a value of 0.23%. In another hand lattice parameter (a) ended up on a stable state with the value of 2.8313 A°.

Scanning Electron Microscope (SEM) examination demonstrated a change in particle size and shape, with a notable reduction in size of the mixture after 15 hours of milling. Energy-dispersive X-ray spectroscopy (EDS) analysis confirmed the presence of both Fe and SiO2 in the resulting nanocomposite.

For $Fe/SiO_2$ magnetic characteristics, vibrating sample magnetometer (VSM) measurements provided insights into its ferromagnetic behavior. The saturation magnetization, Ms, decreased with increasing milling time to a value of 140.79 emu/g after 30 hours. In contrast, the remanence, Mr, and coercivity, Hc, showed enhancement, reaching 7.73 emu/g and 69.07 Oe, respectively. These results underscore the strong and unique magnetic properties of iron when embedded in a silica matrix.

The combination of iron and silica in nanocomposites is regarded as a highly promising combination in the realm of metal matrix nanomaterials. Silica serves as an excellent supporting material for iron as a strong magnetic metal, the magnetic properties of iron nanoparticles can be modified or modified by their interaction with the silica matrix, leading to improved performance in magnetic applications.

Overall, the iron-silica nanocomposite offers an intresting platform for integrating magnetic properties with the benefits of silica as a matrix material, making it suitable for a wide range of applications in the field of nanotechnology.

In the future perspective, we will improve the magnetic properties of $Fe/SiO_2$ nanocomposite by adding other elements or applying annealing treatments. We will utilize other sophisticated characterization techniques such as Transmission Electron Microscopy (TEM), Mössbauer spectroscopy, Atomic Force Microscopy (AFM), and so on to monitor the evolution of these parameters.

# Liste of symbols and abbreviations

| | |
|---|---|
| **1D** | One Dimension |
| **2D** | Two Dimension |
| **3D** | Three Dimension |
| **A** | Vibration Amplitude |
| **a** | The lattice parameters |
| **BPR** | Ball-to-Powder weight Ratio |
| **CMNCs** | Ceramic Matrix NanoComposites |
| **CVD** | Chemical Vapour Deposition |
| **D** | Crystallite size |
| **$d_{hkl}$** | Interreticular Distance |
| **EDS** | Energy Dispersive Spectroscopy |
| **EMF** | Electromotive Force |
| **ECT** | Eddy Current Testing |
| **e.m.f.** | Electromotive Force |
| **FESEM** | Field Emission Scanning Electron Microscopy |
| **FWHM/ β** | Full-Width at Half Maximum |
| **Fe** | Iron |
| **Hc** | Coercivity |
| **HEBM** | High-Energy Ball Milling |
| **MA** | Mechanical Alloying |
| **Ms** | Saturation magnetization |
| **Mr** | Remanence |
| **MMNCs** | Metal Matrix NanoComposites |
| **mm** | Millimeter |
| **NC** | NanoComposites |
| **NPs** | NanoParticles |
| **NNI** | National Nanotechnology Initiative |
| **nm** | Nanometer |
| **PCAs** | Process Control Agent |
| **PM** | Planetary Ball Mill |
| **PVD** | Physical Vapour Deposition |
| **PMNCs** | Polymer Matrix NanoComposites |

| | |
|---|---|
| **rpm** | Ratio per minute |
| **SMCs** | Soft Magnetic Composites |
| **$SiO_2$** | Silica |
| **SEM** | Scanning Electron Microscope |
| **S** | Sensitivity |
| **μm** | micrometer |
| **μ** | Magnetic Permeability |
| **VSM** | Vibrating Sample Magnetometer |
| **V** | Voltage |
| **ω** | Frequency |
| **XRD** | X-Ray Diffraction |
| **θ** | Bragg Angle |
| **λ** | The X-ray Wavelength |
| **ϕ** | Magnetic Flux |
| **δ** | Skin Depth |
| **σ** | Electrical Conductivity |

# References:


[1] Leon, L., Chung, E. J., & Rinaldi, C. A brief history of nanotechnology and introduction to nanoparticles for biomedical applications. In Nanoparticles for Biomedical Applications (pp. 1-4). Elsevier. (2020).

[2] Kumar, R., Kumar, M., & Luthra, G. Fundamental approaches and applications of nanotechnology: A mini review. Materials Today: Proceedings. (2023).

[3] El-Eskandarany, M. S. The history and necessity of mechanical alloying. Mechanical Alloying, 2, 13-47. (2015).

[4] Zhao, Y. W., Zhang, X. K., & Xiao, J. Q. Submicrometer laminated Fe/$SiO_2$ soft magnetic composites—An effective route to materials for high-frequency applications. Advanced Materials, 17(7), 915-918. (2005).

[5] Zhang, X. F., Dong, X. L., Huang, H., Lv, B., Zhu, X. G., Lei, J. P., ... & Zhang, Z. D. Synthesis, structure and magnetic properties of SiO2-coated Fe nanocapsules. Materials Science and Engineering: A, 454, 211-215. (2007).

[6] Thirumal, E., Prabhu, D., Chattopadhyay, K., & Ravichandran, V. Synthesis, magnetic and electrical properties of Fe-containing $SiO_2$ nanocomposite. Journal of alloys and compounds, 502(1), 169-175. (2010).

[7] Jeevanandam, J., Barhoum, A., Chan, Y. S., Dufresne, A., & Danquah, M. K. Review on nanoparticles and nanostructured materials: history, sources, toxicity and regulations. Beilstein journal of nanotechnology, 9(1), 1050-1074. (2018).

[8] Ahire, S. A., Bachhav, A. A., Pawar, T. B., Jagdale, B. S., Patil, A. V., & Koli, P. B. The augmentation of nanotechnology era: A concise review on fundamental concepts of nanotechnology and applications in material science and technology. Results in Chemistry, 100633. (2022).

[9] Yadav, R., Dubey, A., Tiwari, S. P., Shrivastava, P., & Mandal, S. Nanotechnology and its Applications: A Scientific Boon for Future.

[10] Baig, N., Kammakakam, I., & Falath, W. Nanomaterials: A review of synthesis methods, properties, recent progress, and challenges. Materials Advances, 2(6), 1821-1871. (2021).

[11] Twardowski, T. E. Introduction to nanocomposite materials: properties, processing, characterization. DEStech Publications, Inc. (2007).

[12] Pina, S., Oliveira, J. M., & Reis, R. L. Natural-based nanocomposites for bone tissue engineering and regenerative medicine: A review. Advanced Materials, 27(7), 1143-1169. (2015).

[13] Rafiee, M. A., Rafiee, J., Wang, Z., Song, H., Yu, Z. Z., & Koratkar, N. Enhanced mechanical properties of nanocomposites at low graphene content. ACS nano, 3(12), 3884-3890. (2009).

[14] Mariano, M., El Kissi, N., & Dufresne, A. Cellulose nanocrystals and related nanocomposites: Review of some properties and challenges. Journal of Polymer Science Part B: Polymer Physics, 52(12), 791-806. (2014).

[15] Hu, H., Onyebueke, L., & Abatan, A. Characterizing and modeling mechanical properties of nanocomposites-review and evaluation. Journal of minerals and materials characterization and engineering, 9(04), 275. (2010).
[16] Ajayan, P. M. Bulk metal and ceramics nanocomposites. Nanocomposite science and technology, 1-75. (2003).
[17] Lateef, A., & Nazir, R. Metal nanocomposites: Synthesis, characterization and their applications. Sci. Appl. Tailored Nanostructures, 239-256. (2017).
[18] Omanović-Mikličanin, E., Badnjević, A., Kazlagić, A., & Hajlovac, M. Nanocomposites: A brief review. Health and Technology, 10, 51-59. (2020).
[19] Harmer, M. P., Chan, H. M., & Miller, G. A. Unique opportunities for microstructural engineering with duplex and laminar ceramic composites. Journal of the American Ceramic Society, 75(7), 1715-1728. (1992).
[20] Sun, N., Jeurgens, L. P., Burghard, Z., & Bill, J. Ionic liquid assisted fabrication of high performance SWNTs reinforced ceramic matrix nano-composites. Ceramics International, 43(2), 2297-2304. (2017).
[21] Ghasali, E., Yazdani-rad, R., Asadian, K., & Ebadzadeh, T. Production of Al-SiC-TiC hybrid composites using pure and 1056 aluminum powders prepared through microwave and conventional heating methods. Journal of Alloys and Compounds, 690, 512-518. (2017).
[22] Camargo, P. H. C., Satyanarayana, K. G., & Wypych, F. Nanocomposites: synthesis, structure, properties and new application opportunities. Materials Research, 12, 1-39. (2009).
[23] Kobayashi, T. (Ed.). Applied environmental materials science for sustainability. IgI Global. (2016).
[24] Dermenci, K. B., Genc, B., Ebin, B., Olmez-Hanci, T., & Gürmen, S. Photocatalytic studies of Ag/ZnO nanocomposite particles produced via ultrasonic spray pyrolysis method. Journal of alloys and compounds, 586, 267-273. (2014).
[25] Kashinath, L., Namratha, K., & Byrappa, K. Sol-gel assisted hydrothermal synthesis and characterization of hybrid ZnS-RGO nanocomposite for efficient photodegradation of dyes. Journal of Alloys and Compounds, 695, 799-809. (2017).
[26] Ren, Q., Su, H., Zhang, J., Ma, W., Yao, B., Liu, L., & Fu, H. Rapid eutectic growth of $Al_2O_3/Er_3Al_5O_{12}$ nanocomposite prepared by a new method: melt falling-drop quenching. Scripta Materialia, 125, 39-43. (2016).
[27] Abdelhamid, H. N., Talib, A., & Wu, H. F. One pot synthesis of gold–carbon dots nanocomposite and its application for cytosensing of metals for cancer cells. Talanta, 166, 357-363. (2017).
[28] Ogasawara, T., Ishida, Y., Ishikawa, T., & Yokota, R. Characterization of multi-walled carbon nanotube/phenylethynyl terminated polyimide composites. Composites Part A: applied science and manufacturing, 35(1), 67-74. (2004).
[29] Alexandre, M., & Dubois, P. Polymer-layered silicate nanocomposites: preparation, properties and uses of a new class of materials. Materials science and engineering: R: Reports, 28(1-2), 1-63. (2000).

[30] Rehab, A., & Salahuddin, N. Nanocomposite materials based on polyurethane intercalated into montmorillonite clay. Materials Science and Engineering: A, 399(1-2), 368-376. (2005).
[31] Sen, M. Nanocomposite materials. Nanotechnology and the Environment, 1-12. (2020).
[32] Kumar, S. K., & Krishnamoorti, R. Nanocomposites: structure, phase behavior, and properties. Annual review of chemical and biomolecular engineering, 1, 37-58. (2010).
[33] Zheng, X., Forest, M. G., Vaia, R., Arlen, M., & Zhou, R. A strategy for dimensional percolation in sheared nanorod dispersions. Advanced Materials, 19(22), 4038-4043. (2007).
[34] Wong, S., Vaia, R. A., Giannelis, E. P., & Zax, D. B. Dynamics in a poly (ethylene oxide)-based nanocomposite polymer electrolyte probed by solid state NMR. Solid State Ionics, 86, 547-557. (1996).
[35] Hafeez, M. Recent progress and overview of nanocomposites. Nanocomposite Materials. (2022).
[36] Behera, A. Advanced Materials: An Introduction to Modern Materials Science. Springer Nature. (2021).
[37] Behrens, S., & Appel, I. Magnetic nanocomposites. Current opinion in biotechnology, 39, 89-96. (2016).
[38] Coey, J. M. Magnetism and magnetic materials. Cambridge university press. (2010).
[39] Krishnan, K. M. Fundamentals and applications of magnetic materials. Oxford University Press. (2016).
[40] Cullity, B. D., & Graham, C. D. Introduction to magnetic materials. John Wiley & Sons. (2011).
[41] Biswas, A., Bayer, I. S., Biris, A. S., Wang, T., Dervishi, E., & Faupel, F. Advances in top–down and bottom–up surface nanofabrication: Techniques, applications & future prospects. Advances in colloid and interface science, 170(1-2), 2-27. (2012).
[42] Arole, V. M., & Munde, S. V. Fabrication of nanomaterials by top-down and bottom-up approaches-an overview. J. Mater. Sci, 1, 89-93. (2014).
[43] Rane, A. V., Kanny, K., Abitha, V. K., & Thomas, S. Methods for synthesis of nanoparticles and fabrication of nanocomposites. In Synthesis of inorganic nanomaterials (pp. 121-139). Woodhead publishing. (2018).
[44] Basset, D., Miani, F., & Le Caer, G. Mechanosynthesis of nanophase materials. Nanostructured materials, 2(3), 217-229. (1993).
[45] El-Eskandarany, M. S., Al-Hazza, A., Al-Hajji, L. A., Ali, N., Al-Duweesh, A. A., Banyan, M., & Al-Ajmi, F. Mechanical milling: A superior nanotechnological tool for fabrication of nanocrystalline and nanocomposite materials. Nanomaterials, 11(10), 2484. (2021).
[46] Suryanarayana, C., Al-Joubori, A. A., & Wang, Z. Nanostructured materials and nanocomposites by mechanical alloying: An overview. Metals and Materials International, 28(1), 41-53. (2022).
[47] Yadav, T. P., Yadav, R. M., & Singh, D. P. Mechanical milling: a top down approach for the synthesis of nanomaterials and nanocomposites. Nanoscience and Nanotechnology, 2(3), 22-48. (2012).

[48] Benjamin, J. S., & Volin, T. E. The mechanism of mechanical alloying. Metallurgical Transactions, 5, 1929-1934. (1974).
[49] Murty, B. S., & Ranganathan, S. J. M. R. Novel materials synthesis by mechanical alloying/milling. International materials reviews, 43(3), 101-141. (1998).
[50] Koch, C. C. Materials synthesis by mechanical alloying. Annual review of materials science, 19(1), 121-143. (1989).
[51] Harris, K. D. How grinding evolves. Nature chemistry, 5(1), 12-14. (2013).
[52] Friščić, T., Halasz, I., Beldon, P. J., Belenguer, A. M., Adams, F., Kimber, S. A., ... & Dinnebier, R. E. Real-time and in situ monitoring of mechanochemical milling reactions. Nature chemistry, 5(1), 66-73. (2013).
[53] Mhadhbi, M. Modelling of the High-Energy Ball Milling Process. Advances in Materials Physics and Chemistry, 11(1), 31-44. (2021).
[54] Suryanarayana, C. Mechanical alloying and milling. Progress in materials science, 46(1-2), 1-184. (2001).
[55] Kopp Alves, A., Bergmann, C. P., Berutti, F. A., Kopp Alves, A., Bergmann, C. P., & Berutti, F. A. High-energy milling. Novel synthesis and characterization of nanostructured materials, 77-85. (2013).
[56] Suryanarayana, C. Does a disordered γ-TiAl phase exist in mechanically alloyed TiAl powders?. Intermetallics, 3(2), 153-160. (1995).
[57] Calka, A., & Williams, J. S. Synthesis of nitrides by mechanical alloying. In Materials Science Forum (Vol. 88, pp. 787-794). Trans Tech Publications Ltd. (1992).
[58] Chen, Y., & Williams, J. R. Hydriding reactions induced by ball milling. In Materials Science Forum (Vol. 225, pp. 881-888). Trans Tech Publications Ltd. (1996).
[59] Hwang, S. J., Nash, P., Dollar, M., & Dymek, S. Microstructure and mechanical properties of mechanically alloyed NiAl. MRS Online Proceedings Library (OPL), 213. (1990).
[60] Huang, B. L., Perez, R. J., Crawford, P. J., Nutt, S. R., & Lavernia, E. J. The synthesis of nanocrystalline Fe78B13Si9 by cryogenic high-energy ball milling of metglas. Nanostructured materials, 7(1-2), 57-65. (1996).
[61] Chin, Z. H., & Perng, T. P.. Amorphization of Ni-Si-C ternary alloy powder by mechanical alloying. In Materials Science Forum (Vol. 235, pp. 121-126). Trans Tech Publications Ltd. (1996, October)
[62] Kis-Varga, M., & Beke, D. L. Phase transitions in Cu-Sb systems induced by ball milling. In Materials science forum (Vol. 225, pp. 465-470). Aedermannsdorf, Switzerland: Trans Tech Publications, 1984-.(1996, July).
[63] de Julián, C., Alcázar, G. P., Cebollada, F., Montero, M. I., González, J. M., & Marco, J. F. Mössbauer analysis of the phase distribution present in nanoparticulate Fe/SiO2 samples. Journal of magnetism and magnetic materials, 203(1-3), 175-177. (1999).
[64] Xiong, C., Yu, K. N., & Xiong, Y. The microstructure and magnetic properties of nanocomposite Fex (SiO2) 1-x materials. Nanostructured materials, 11(4), 477-486. (1999).
[65] Alonso-Sanudo, M., Blackwell, J. J., O'Grady, K., González, J. M., Cebollada, F., & Morales, M. P. Magnetic behaviour and percolation in mechanically alloyed Fe–$SiO_2$

granular solids. Journal of magnetism and magnetic materials, 221(1-2), 207-214. (2000).

[66] Blackwell, J. J., Morales, M. P., O'Grady, K., González, J. M., Cebollada, F., & Alonso-Sañudo, M. Interactions and hysteresis behaviour of $Fe/SiO_2$ nanocomposites. Journal of magnetism and magnetic materials, 242, 1103-1105. (2002).

[67] López, G. P., & Silvetti, S. P. Effect of milling time on $Fe/SiO_2$ system prepared by mechanical alloying. Physica B: Condensed Matter, 354(1-4), 141-144. (2004).

[68] Yan, L., Wang, J., Han, X., Ren, Y., Liu, Q., & Li, F. Enhanced microwave absorption of Fe nanoflakes after coating with SiO2 nanoshell. Nanotechnology, 21(9), 095708. (2010).

[69] Lomaeva, S. F., Maratkanova, A. N., Nemtsova, O. M., Chulkina, A. A., Bokhonov, B. B., Ancharov, A. I., & Elsukov, E. P. The formation of structure and phase composition and magnetic properties of Fe ($Fe_3C$, $Fe_5SiC$)-$SiO_2$ nanocomposites upon mechanical alloying. The Physics of Metals and Metallography, 109, 534-546. (2010).

[70] Ahmad, T., Mamat, O., & Ahmad, R. Physico-Mechanical Properties of Sintered Iron-Silica Sand Nanoparticle Composites: a Preliminary Study. In Defect and Diffusion Forum (Vol. 332, pp. 7-16). Trans Tech Publications Ltd. (2012).

[71] Lopez, G. P., Condó, A. M., Urreta, S. E., & Silvetti, S. P. Synthesis of $Fe/SiO_2$ and iron oxides/$SiO_2$ nanocomposites by long-term ball milling. Materials Research Bulletin, 49, 237-244. (2014).

[72] Rudeichuk, T., Maciazsek, R., Onderko, F., Tkac, M., & Oleksakova, D. influence of ball to powder ratio at mechanical milling on the coercivity of soft magnetic composites.

[73] Vovk, S., Dobák, S., Füzer, J., Kollár, P., Bureš, R., & Fáberová, M. Loss separation and thermal studies of Fe/SiO2/ferrite soft magnetic composites. Journal of Alloys and Compounds, 945, 169254. (2023).

[74] White, W. M., Casey, W. H., & Marty, B. Encyclopedia of geochemistry: a comprehensive reference source on the chemistry of the earth. (No Title). (2018).

[75] Pepperhoff, W., & Acet, M. Constitution and Magnetism of Iron and its Alloys. Springer Science & Business Media. (2001).

[76] Flörke, O. W., Graetsch, H. A., Brunk, F., Benda, L., Paschen, S., Bergna, H. E., ... & Schiffmann, D. Silica, Ullmann's encyclopedia of industrial chemistry. (2008).

[77] Griscom, D. L. The electronic structure of $SiO_2$: a review of recent spectroscopic and theoretical advances. Journal of Non-Crystalline Solids, 24(2), 155-234. (1977).

[78] N'Tsouaglo, K. G. Caratérisation de la surface d'énergie potentielle des matériaux complexes et son application sur la cinétique du $SiO_2$/Si. (2015).

[79] Fatimah, I., Fadillah, G., Purwiandono, G., Sahroni, I., Purwaningsih, D., Riantana, H., ... & Sagadevan, S. Magnetic-silica nanocomposites and the functionalized forms for environment and medical applications: A review. Inorganic Chemistry Communications, 109213. (2022).

[80] Corrias, A., Ennas, G., Paschina, G., Piccaluga, G., & Zedda, D. Mechanosynthesis of metal-silica nanocomposites. In Materials Science Forum (Vol. 195, pp. 25-30). Trans Tech Publications Ltd. (1995).

[81] Retsch GmbH - www.retsch.com (2023) (PLANETARY BALL MILL PM 400)
[82] Bokobza, L. Spectroscopic techniques for the characterization of polymer nanocomposites: a review. Polymers, 10(1), 7. (2017).
[83] Akhtar, K., Khan, S. A., Khan, S. B., & Asiri, A. M. Scanning electron microscopy: Principle and applications in nanomaterials characterization. Handbook of materials characterization, 113-145. (2018).
[84] Mohammed, A., & Abdullah, A. Scanning electron microscopy (SEM): A review. In Proceedings of the 2018 International Conference on Hydraulics and Pneumatics—HERVEX, Băile Govora, Romania (Vol. 2018, pp. 7-9). (2018, November).
[85] Zhou, W., & Wang, Z. L. (Eds.). Scanning microscopy for nanotechnology: techniques and applications. Springer science & business media. (2007).
[86] Nasrazadani, S., & Hassani, S. Modern analytical techniques in failure analysis of aerospace, chemical, and oil and gas industries. Handbook of materials failure analysis with case studies from the oil and gas industry, 39-54. (2016).
[87] Gibson, L. T., Worsfold, P. J., Townshend, A., & Poole, C. F. Archaeometry and antique analysis:(b) metallic and ceramic objects. In Encyclopedia of Analytical Science (pp. 117-123). Elsevier Limited. (2004).
[88] Gumustas, M., Sengel-Turk, C. T., Gumustas, A., Ozkan, S. A., & Uslu, B. Effect of polymer-based nanoparticles on the assay of antimicrobial drug delivery systems. In Multifunctional systems for combined delivery, biosensing and diagnostics (pp. 67-108). Elsevier. (2017).
[89] Tan, W. L., & McNeill, C. R. X-ray diffraction of photovoltaic perovskites: Principles and applications. Applied Physics Reviews, 9(2), 021310. (2022).
[90] Epp, J. X-ray diffraction (XRD) techniques for materials characterization. In Materials characterization using nondestructive evaluation (NDE) methods (pp. 81-124). Woodhead Publishing. (2016).
[91] Thomas, S., & Nochehdehi, A. R. (Eds.). Handbook of Magnetic Hybrid Nanoalloys and Their Nanocomposites. Springer Nature. (2022).
[92] Franco, V., & Dodrill, B. (Eds.). Magnetic measurement techniques for materials characterization. Springer International Publishing. (2021).
[93] Thomson, T. Magnetic properties of metallic thin films. Metallic films for electronic, optical and magnetic applications, 454-546. (2014).
[94] Ida, N., & Meyendorf, N. (Eds.). Handbook of advanced nondestructive evaluation (pp. 235-251). Cham, Switzerland: Springer International Publishing. (2019).
[95] Sophian, A., Tian, G. Y., Taylor, D., & Rudlin, J. Electromagnetic and eddy current NDT: a review. Insight, 43(5), 302-306. (2001).
[96] Das, R., Ali, E., & Abd Hamid, S. B. current applications of x-ray powder diffraction-a review. Reviews on Advanced Materials Science, 38(2). (2014).
[97] Soni, R. A., Rana, R. S., & Godara, S. S. Characterization Tools and Techniques for Nanomaterials and Nanocomposites. In Nanomaterials and Nanocomposites (pp. 61-83). CRC Press. (2021).
[98] Vives, S., Gaffet, E., & Meunier, C. X-ray diffraction line profile analysis of iron ball milled powders. Materials Science and Engineering: A, 366(2), 229-238. (2004).

[99] Lomayeva, S. F., Maratkanova, A. N., Rozanov, K. N., Petrov, D. A., & Yelsukov, E. P. Structure, Magnetic and Microwave Properties of Granular $Fe_x$ $(SiO_2)$ $_{1-x}$ Alloys Obtained by Mechanochemical Synthesis. In Solid State Phenomena (Vol. 190, pp. 585-588). Trans Tech Publications Ltd. (2012).

[100] Rane, G. K., Welzel, U., Meka, S. R., & Mittemeijer, E. J. Non-monotonic lattice parameter variation with crystallite size in nanocrystalline solids. Acta Materialia, 61(12), 4524-4533. (2013).

[101] Klug, H. P., & Alexander, L. E. X-ray diffraction procedures: for polycrystalline and amorphous materials (p. 992). (1974).

[102] Zou, B. F., Zhou, T. D., & Hu, J. Effect of amorphous evolution on structure and absorption properties of FeSiCr alloy powders. Journal of magnetism and magnetic materials, 335, 17-20. (2013).

[103] Khani, O., Shoushtari, M. Z., Ackland, K., & Stamenov, P. The structural, magnetic and microwave properties of spherical and flake shaped carbonyl iron particles as thin multilayer microwave absorbers. Journal of Magnetism and Magnetic Materials, 428, 28-35. (2017).

[104] Thanh Ho, V. T., Hong, N. V. H., Van Nguyen, A., Bach, L. G., & Dinh, T. P. Core–Shell Fe@ $SiO_2$ Nanoparticles Synthesized via Modified Stober Method for High Activity in Cr (VI) Reduction. Journal of Nanoscience and Nanotechnology, 18(10), 6867-6872. (2018).

[105] Zhang, H., Yin, Y., Gao, L., & Wei, G. Improved Microwave Absorbing Performance in High Frequency Range of Iron Nanoparticles After Coating by $SiO_2$ Nanoshell. Journal of Electronic Materials, 49, 6428-6435. (2020).